© 2014. Published by The Company of Biologists Ltd | Development (2014) 141, 3212-3221 doi:10.1242/dev.102541

RESEARCH ARTICLE

Kremen1 restricts Dkk activity during posterior lateral line development in zebrafish

Hillary F. McGraw, Maya D. Culbertson* and Alex V. Nechiporuk‡

ABSTRACT

Canonical Wnt signaling plays crucial roles during development and disease. How Wnt signaling is modulated in different *in vivo* contexts is currently not well understood. Here, we investigate the modulation of Wnt signaling in the posterior lateral line primordium (pLLP), a cohort of ~100 cells that collectively migrate along the trunk of the zebrafish embryo. The pLLP comprises proliferative progenitor cells and organized epithelial cells that will form the mechanosensory organs of the posterior lateral line. Wnt signaling is active in the leading progenitor zone of the pLLP and restricted from the trailing zone through expression of the secreted Wnt inhibitors *dkk1b* and *dkk2*. We have identified a zebrafish strain, *krm1*^{nl10}, which carries a mutation in the *kremen1* gene, a non-obligate co-receptor for the Dkk family of proteins. Previous studies have shown that Kremen1 inhibits Wnt signaling by facilitating internalization of the Kremen1-Dkk-Lrp5/6 complex. Surprisingly, we found that disruption of Kremen1 in the pLLP exhibited molecular and cellular phenotypes associated with a decrease rather than overactivation of Wnt signaling. Transplantation of wild-type cells into the mutant primordia failed to rescue the *krm1*^{nl10} phenotype, thus revealing that the effects of Kremen1 loss are non-cell-autonomous. Finally, ectopic expression of Dkk1b-mTangerine protein revealed larger spread of the fusion protein in the mutant primordia compared with the wild type. Based on our data, we propose a novel mechanism in which Kremen1 modulates Wnt activity by restricting the range of secreted Dkk proteins during collective cell migration in the pLLP.

KEY WORDS: Dkk, Kremen1, Lateral line, Wnt, Zebrafish

INTRODUCTION

Canonical Wnt signaling regulates many cellular behaviors during embryonic development, such as progenitor cell maintenance, proliferation, migration and differentiation (Grigoryan et al., 2008). The canonical Wnt signaling pathway is activated by a large family of secreted Wnt ligands that bind to Frizzled receptor and LDL receptor-related proteins 5 and 6 (Lrp5/6). The single-pass transmembrane proteins Kremen1 and Kremen2 have been identified as modulators of canonical Wnt signaling (Cselenyi and Lee, 2008; Nakamura et al., 2008). Kremen1/2 are high-affinity co-receptors for Dickkopf (Dkk) proteins, a family of secreted Wnt inhibitors. During development of various organs, including the nervous system, limbs and liver, Kremen1/2 synergize with the Dkk proteins to inhibit Wnt signaling (Davidson et al., 2002; Ellwanger et al., 2008; Lu et al., 2013). Dkk inhibits Wnt activity by competitively binding to Lrp5/6. In cultured cells, Dkk binds to Kremen1/2 and Lrp5/6, thereby forming a protein complex; this ternary complex is endocytosed and probably targeted for degradation (Nakamura et al., 2008). Studies in mice and *Xenopus* demonstrated that Dkk binding to Kremen1/2 inhibits canonical Wnt signaling, as loss of Kremen1/2 function leads to Wnt overactivation phenotypes, such as defects in anterior CNS development and limb formation (Davidson et al., 2002; Osada et al., 2006; Ellwanger et al., 2008). Furthermore, in zebrafish, Dkk and Kremen1 (a Kremen2 homolog has not been identified in zebrafish) have been shown to regulate mechanosensory organ size by inhibiting Wnt mediated proliferation (Wada et al., 2013). By contrast, in the absence of Dkk, Kremen1/2 were found to bind directly to Lrp5/6 *in vitro*, and Kremen2 facilitates Wnt activity during neural crest induction in *Xenopus* (Hassler et al., 2007). Further research is required to more fully elucidate how Kremen1/2 modulate canonical Wnt signaling during development *in vivo*.

The zebrafish posterior lateral line (pLL) mechanosensory system has proven to be an excellent model for studying how Wnt/β-catenin signaling regulates cellular dynamics during embryonic development. Formation of the pLL occurs through the collective migration of a cohort of ~100 cells called the pLL primordium (pLLP) (Aman and Piotrowski, 2009; Chitnis et al., 2012). As the pLLP migrates, it deposits patterned clusters of cells that will form mechanosensory organs called neuromasts (NMs). As each maturing NM is deposited from the rostral (trailing) region of the pLLP, proliferating progenitor cells in the caudal (leading) region of the pLLP give rise to new proto-NMs. At the end of pLLP migration, the nascent pLL consists of 5-6 NMs along the trunk of the zebrafish embryo and a terminal cluster (tc) of 2-3 NMs at the end of the tail.

The Wnt/β-catenin and Fgf signaling pathways interact to regulate cellular proliferation, differentiation and migration in the pLLP (Aman and Piotrowski, 2009; Chitnis et al., 2012; Harding and Nechiporuk, 2012). Canonical Wnt signaling is active in the leading region of the pLLP and restricted in the trailing zone, in part by expression of *dkk1b* (Aman and Piotrowski, 2008). Conditional overexpression of *dkk1b* results in a dramatic truncation in the pLL due to loss of pLLP organization, decreased cellular proliferation, increased cell death and failed migration (Aman and Piotrowski, 2008; Aman et al., 2011; McGraw et al., 2011). The Fgf signaling pathway is active in the mid-region of the pLLP and is required for the formation of proto-NMs (Aman and Piotrowski, 2009; Chitnis et al., 2012; Harding and Nechiporuk, 2012). Recent work by Matsuda et al. (2013) showed that Wnt signaling through Lymphoid enhancer-binding factor 1 (*lef1*) regulates NM spacing along the trunk through the expression of the Fgf pathway inhibitor Dual specificity phosphatase 6 (*dusp6*) in the leading region of the pLLP (Matsuda et al., 2013). In summary, the Wnt pathway must be precisely regulated in the pLLP to ensure proper pLL development.

Oregon Health & Science University, Department of Cell and Developmental Biology, Portland, OR 97239, USA.
*Present address: Maimonides Medical Center, Department of Orthopedic Surgery, Brooklyn, NY 11219, USA.

‡Author for correspondence (nechipor@ohsu.edu)

Received 21 August 2013; Accepted 17 June 2014

Development (2014) 141, 3212-3221 doi:10.1242/dev.102541

In this study, we show that Kremen1 acts in the pLLP to modulate Wnt signaling. We have identified a *kremen1* mutant strain (*krm1*^{nl10}) that displays a premature and progressive loss of Wnt activity in the leading region of the pLLP, as well as decreased cellular proliferation and increased cell death. Our mosaic analysis revealed that mutation of *kremen1* leads to non-cell-autonomous defects in the pLLP that are morphologically similar to ectopic activation of Dkk1 (McGraw et al., 2011). Attenuating Dkk levels, either by morpholino knockdown of *dkk1b/2* or inhibition of Fgf signaling, results in a partial rescue of the *krm1*^{nl10} phenotype. Analysis of tagged Dkk1b protein in *krm1*^{nl10} and wild-type (WT) embryos revealed a broader spread of Dkk1b in mutant primordia. Based on these data, we propose that an absence of Kremen1 function leads to an expanded range of the Dkk signal and, consequently, premature attenuation of Wnt signaling in the pLLP. Our study provides new insight into Kremen1-mediated modulation of Wnt activity *in vivo* during organogenesis and suggests a pathway that might be misregulated during disease.

RESULTS

Kremen1 is required for pLL formation

In an ongoing N-ethyl-N-nitrosourea (ENU)-based screen to identify zebrafish mutants with defects in pLL development, we isolated the strain *krm1*^{nl10}. By contrast to complete pLLP migration in WT embryos, migration of the pLLP halted midway along the trunk in *krm1*^{nl10} mutants, and the pLLP dispersed into a single line of cells extending from the last deposited NM (Fig. 1A,B). Live imaging demonstrated that new NM deposition failed in the caudal portion of the trunk due to a failure of proto-NM renewal in mutant primordia (Fig. 1E,F; supplementary material Movies 1, 2). As a result, by 2 days post fertilization (dpf), *krm1*^{nl10} mutants showed significantly fewer NMs that were also shifted anteriorly, and an invariable lack of tc NMs (Fig. 1A,B,D,G). Adult *krm1*^{nl10} homozygous mutants were viable, mated naturally and produced offspring, although they lacked NMs on the caudal-most trunk and tail as adults (supplementary material Fig. S1A,B).

Positional cloning of the *krm1*^{nl10} mutation identified a single base pair change from thymine to cytosine in the splice donor site of intron 6 of the *kremen1* gene on chromosome 5 (supplementary material Fig. S2A,B). RT-PCR for *kremen1* generated a single product in WT embryos and at least two variants in *krm1*^{nl10} mutants (supplementary material Fig. S2C,D). Variant 1, the more abundant product, resulted from improper splicing and insertion of the 100 base pair (bp) intron 6 between exons 6 and 7. Variant 2 resulted from premature splicing of exon 7, which led to the loss of 31 bp in exon 6 (supplementary material Fig. S2D). Both variants contained predicted translational frame shifts, which resulted in premature stop codons and disruption of the CUB domain, an essential domain for Kremen1/Dkk binding (Mao et al., 2002), and in loss of the transmembrane domain (supplementary material Fig. S2E). Injection of 200 pg/nl WT *kremen1* mRNA rescued the loss of tc NMs in *krm1*^{nl10} mutants without producing obvious loss of Wnt phenotypes in WT embryos. By contrast, expression of mRNA encoding mutant variants 1 or 2 failed to rescue tc NMs in *krm1*^{nl10} mutant embryos (supplementary material Fig. S2G). Injection of *kremen1* morpholino antisense oligonucleotide (*krm1*-MO) (Gore et al., 2011), along with *p53*-MO to minimize non-specific cell death (Robu et al., 2007), into WT *Tg(cldnB:GFP)* zygotes produced embryos missing tc NMs and an anterior shift in the axial level of deposited NMs, phenotypes similar to those observed in *krm1*^{nl10} mutants (Fig. 1B,C,D,G). Together, these data indicate that the *krm1*^{nl10} mutant phenotype results from a loss of Kremen1 function.

kremen1, *dkk1b*/*2* and *lrp5*/*6* are expressed in the pLLP

At 30 hours post fertilization (hpf), *kremen1* was expressed in discrete regions in the developing embryo, including the pLLP, lens,

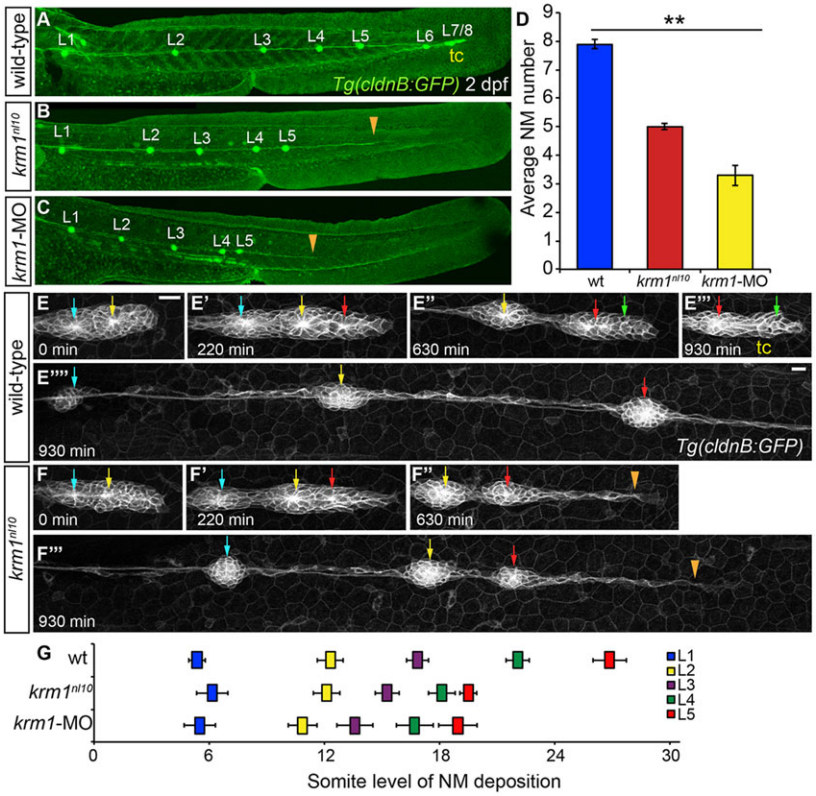

Fig. 1. The pLL is truncated in *krm1*^{nl10} mutants. (A-C) Confocal projections of 2 dpf larvae expressing *Tg(cldnB:GFP)*, (L1-L8: pLL NMs 1-8). (A) WT embryo showing completed pLLP migration and deposition of all NMs. (B) In a *krm1*^{nl10} mutant, there are fewer deposited NMs and the pLLP stalled prematurely (orange arrowhead). (C) *kremen1* morphants show a similar reduction of NMs and pLLP stalling (orange arrowhead). (D) Quantification of neuromasts in WT, *krm1*^{nl10} mutant and *krm1*-MO-injected embryos (n=10 embryos per condition; **P<0.001, one-way ANOVA). (E-F‴) Still confocal projections from live 930-min time-lapse movies showing pLLP migration in WT and *krm1*^{nl10} embryos beginning at 36 hpf. At 0 min, WT and mutant primordia contain two proto-NMs (E,F, blue and yellow arrows). By 220 min, both WT and mutant primordia have added an additional proto-NM (E′,F′, red arrow). (E″) At 630 min, the WT pLLP contains the proto-NMs that will form the terminal cluster (green arrow). By contrast, the *krm1*^{nl10} pLLP fail to form a new proto-NM and migrate as a thin trail of cells (F″, orange arrowhead). By 930 min, WT pLLP has migrated out of frame (E⁗) and formed the tc (E‴). The mutant pLLP has stalled (a thin trail of cells extended from the last deposited NM, marked by orange arrowhead; F‴). (G) Quantification of L1-L5 NM location based on somite level (tc is not included). NMs are shifted anteriorly in *krm1*^{nl10} mutant and *krm1-MO*rphants relative to WT embryos (n=6 embryos per condition; P<0.001, two-way ANOVA with replication). Scale bars: 20 µm. NM, neuromast; tc, terminal cluster.

Development (2014) 141, 3212-3221 doi:10.1242/dev.102541

otic vesicle, midbrain-hindbrain boundary and the nascent tail fin fold (supplementary material Fig. S3A). The Kremen1 ligands *dkk1b* and *dkk2* displayed complementary expression patterns to *kremen1* in the developing embryo (supplementary material Fig. S3B,C). At 32 hpf, *kremen1* was expressed in the leading and mid-zones of WT and *krm1*^{nl10} pLLP (Fig. 2A,B). By 40 hpf, *kremen1* expression was restricted to the leading zone (Fig. 2C,D). We found that, in addition to the previously reported expression of *dkk1b* (Aman and Piotrowski, 2008), *dkk2* was also expressed in the migrating pLLP. In WT embryos, both *dkk1b* and *dkk2* were expressed in the mid-region of the pLLP between 32 and 40 hpf (Fig. 2E,G,I,K). *dkk1b* and *dkk2* had similar expression domains in *krm1*^{nl10} primordia (Fig. 2F,H,J,L). By 40 hpf, *dkk2* was primarily localized at the last deposited NM, and faint expression was present throughout the mutant pLLP, probably due to a loss of proper patterning in the mutant pLLP during late stages of migration (Fig. 2L). In addition, the Wnt and Dkk receptors *lrp5* and *lrp6* were expressed throughout the pLLP at 36 hpf (supplementary material Fig. S4A,B). In summary, the expression domains of *kremen1*, *dkk1b*, *dkk2*, *lrp5* and *lrp6* are consistent with their roles in modulating canonical Wnt activity in the pLLP.

Cellular proliferation and survival are impaired in *krm1*^{nl10} pLLP

Studies in mice and frogs have demonstrated that Kremen1 functions as an inhibitor of canonical Wnt signaling, and loss of Kremen1 function would therefore be expected to result in a Wnt overactivation phenotype (Nakamura et al., 2008). Zebrafish *apc*^{mcr} mutants showed elevated Wnt/β-catenin activity that resulted in increased cellular proliferation and abnormal pLLP migration (Aman and Piotrowski, 2008; Aman et al., 2011). Surprisingly, rather than resembling a Wnt overactivation phenotype, the *krm1*^{nl10} pLL phenotype was strikingly similar to the loss of Wnt signaling found in *lef1* mutants (McGraw et al., 2011; Valdivia et al., 2011). *lef1* mutant primordia showed premature loss of pLLP organization and truncation of the pLL, due in part to a decrease of proliferative cells in the leading region of the pLLP. Thus, we asked whether cell proliferation is impaired in *krm1*^{nl10} mutant primordia.

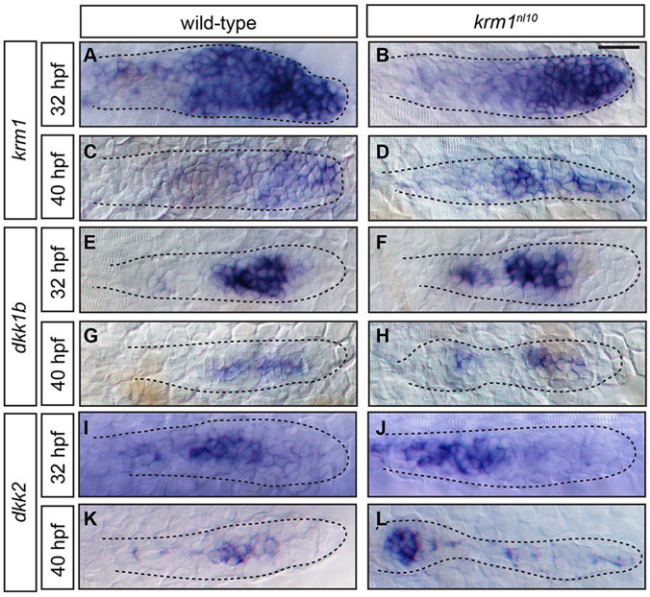

Fig. 2. *kremen1*, *dkk1b* and *dkk2* are expressed in the pLLP of WT and *krm1*^{nl10} mutant embryos. (A-L) Expression of *kremen1*, *dkk1b* and *dkk2* in the primordia (highlighted by dashed lines) of WT and *krm1*^{nl10} embryos at 32 and 40 hpf. *kremen1* expression is progressively decreased and restricted to the leading zone between 32 and 40 hpf in WT (A,C) and *krm1*^{nl10} (B,D) embryos. *dkk1b* is expressed in the mid-zone of the pLLP at 32 and 40 hpf in WT (E,G) and *krm1*^{nl10} (F,H) embryos. *dkk2* is expressed in the mid-zone at 32 hpf in WT (I) and mutant (J) primordia. At 40 hpf, *dkk2* is expressed in the mid-zone of WT pLLP (K) and in the last deposited NM in mutant embryos; faint expression is present throughout the mutant pLLP (L). Scale bar: 20 µm.

Using a bromodeoxyuridine (BrdU) incorporation assay, we found that proliferation was reduced in *krm1*^{nl10} mutant pLLP compared with WT at 34 hpf (Fig. 3A-C). We also observed a significant increase in cell death in *krm1*^{nl10} primordia at 40 hpf using a terminal deoxynucleotidyl transferase dUTP nick end labeling (TUNEL) assay (17.1% TUNEL-positive primordia in WT embryos versus 40.0% in *krm1*^{nl10}; Fig. 3D-F) and caspase immunoreactivity (13% of WT and 27% of mutant primordia showed increased caspase3 immunolabeling; supplementary material Fig. S5A-C). Interestingly, injection of the p53-MO did not rescue NM numbers or spacing in *krm1*^{nl10} mutants compared with uninjected mutant embryos (supplementary material Fig. S11E), suggesting that the loss of proliferation, but not a p53-dependent cell death, is a major cause of the *krm1*^{nl10} phenotype.

To further define the cellular mechanisms underlying the *krm1*^{nl10} phenotype, we used photoconversion of the Kaede fluorophore to mark cells in the leading zone of pLLP at 24 hpf, and then examined their number and location at 48 hpf, when pLLP migration was complete. In WT embryos, labeled cells underwent multiple cell divisions (Fig. 3G,I,K) and populated the terminal NMs. In *krm1*^{nl10} embryos, there was no significant change in the number of labeled cells between 24 and 48 hpf (Fig. 3H,J,K). This result was strikingly different from the behavior of labeled progenitor cells in *lef1*^{nl2} mutants, which remained proliferative but prematurely exited the leading region (McGraw et al., 2011). Thus, *krm1*^{nl10} mutants more closely resemble a phenotype resulting from a global inhibition of Wnt activity by ectopic Dkk1b expression (Aman et al., 2011; McGraw et al., 2011) rather than loss of Wnt transcriptional activity seen in *lef1*^{nl2} mutants.

Wnt activity is prematurely and progressively decreased in *krm1*^{nl10} primordia

Because decreased proliferation and increased cell death are consistent with reduced Wnt signaling, we asked whether expression domains of Wnt target genes, *lef1*, *axin2* and *sef* (Aman and Piotrowski, 2008), were altered in *krm1*^{nl10} mutant pLLPs. At 32 hpf, WT and *krm1*^{nl10} pLLPs showed similar expression patterns for *lef1*, *axin2* and *sef* (Fig. 4A,B,G,H,M,N; Table 1). By 40 hpf, WT primordia displayed a reduction in expression of Wnt target genes, consistent with previous research showing that Wnt signaling was progressively decreased in the pLLP over the course of its migration (Valdivia et al., 2011; Matsuda et al., 2013). By contrast, *krm1*^{nl10} primordia showed an earlier reduction of target gene expression at 36 hpf and an even more substantial reduction by 40 hpf (Fig. 4D,F,J,L,P,R; Table 1).

To further investigate modulation of Wnt activity in *krm1*^{nl10} mutants, we used a transgenic biosensor line, *Tg(7xtcf-siam:eGFP)*, which responds to Wnt/β-catenin activity (Valdivia et al., 2011; Moro et al., 2012). At 36 hpf, WT embryos showed GFP-positive cells predominantly in the leading region of the pLLP (supplementary material Fig. S6A-A″). By contrast, in *krm1*-MO-injected embryos, the number of GFP-positive cells was significantly decreased in the leading region of the pLLP (supplementary material Fig. S6B-B″,F), although the overall number of GFP-positive cells was not significantly different from WT (supplementary material Fig. S6E). By 40 hpf, GFP was significantly downregulated throughout the

Development (2014) 141, 3212-3221 doi:10.1242/dev.102541

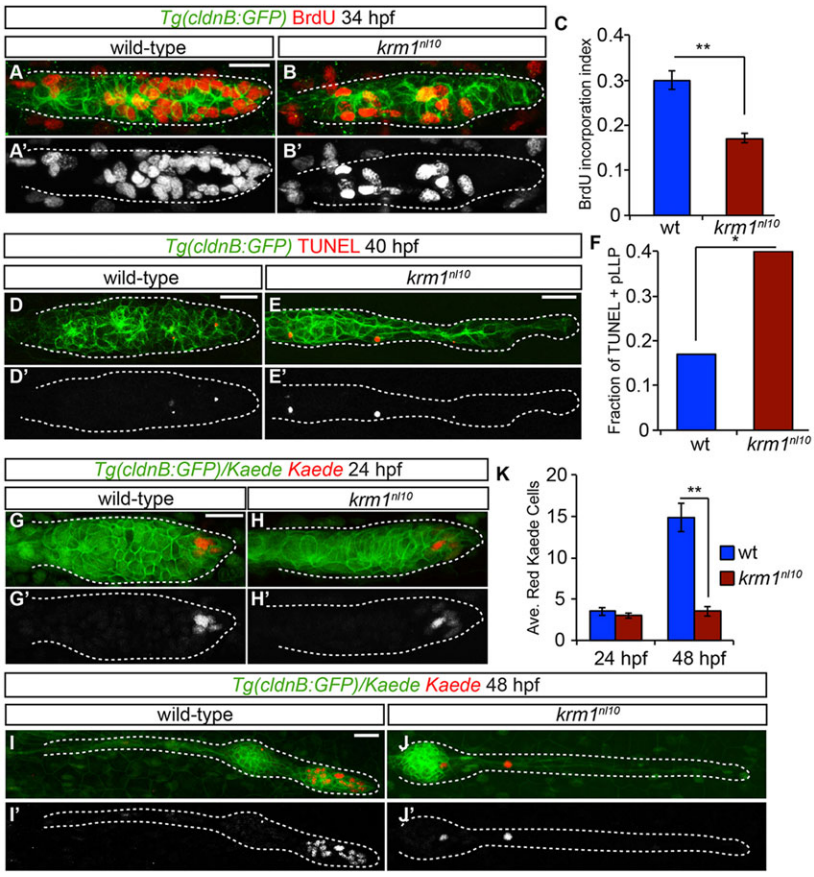

Fig. 3. Cellular proliferation and survival are impaired in *krm1*^{nl10} pLLP. (A-B′) BrdU incorporation in WT and *krm1*^{nl10} primordia between 32.5 and 34 hpf. (C) Quantification of cells that have incorporated BrdU, showing a significant decrease in *krm1*^{nl10} mutant embryos versus WT (n=10 WT and 9 mutant embryos; **P<0.001, Student's t-test). (D-E′) Confocal projections of pLLP at 40 hpf labeled with TUNEL (red) in *Tg(cldnB:GFP)*+ (green) in WT (D,D′) and *krm1*^{nl10} (E,E′) embryos. (F) TUNEL-positive fractions of pLLPs. Significantly more *krm1*^{nl10} mutant pLLPs contained TUNEL-positive puncta (n=35 WT and 40 mutant embryos; *P<0.03, Fisher's Exact Test). (G-J′) Confocal projections of live *Tg(cldnB:GFP)* (green) embryos at 24 hpf labeled with nuclear-localized Kaede before (green) and after (red) photoconversion. At 24 hpf, both WT (G,G′) and *krm1*^{nl10} (H,H′) embryos contain photoconverted Kaede cells in the leading zone of the pLLP. At 48 hpf, photoconverted Kaede cells in the WT embryo have divided and are localized in the tc NMs (I,I′). In the *krm1*^{nl10} embryo, photoconverted cells have not proliferated (J,J′). (K) Quantification of photoconverted Kaede cells at 24 and 48 hpf; there are significantly fewer converted cells at 48 hpf in *krm1*^{nl10} mutant pLLP compared with WT (n=24 WT and 15 *krm1*^{nl10} mutant embryos; **P<0.001, Student's t-test). Scale bars: 20 µm.

primordia of *kremen1* morphants compared with WT embryos (supplementary material Fig. S6C-F). GFP-positive cells in the trailing and mid-region of morphant primordia at 40 hpf are localized at proto-NMs (supplementary material Fig. S6D-D″, yellow arrows). The fluorescent intensity of GFP expression was significantly reduced in morphant primordia compared with WT at both 36 and 40 hpf (supplementary material Fig. S6E). Together with decreased Wnt target expression, these results indicate a significant decline in Wnt activity in the leading region of the pLLP during later stages of mutant pLL formation.

Recent work has shown that expression of the ERK inhibitor *dusp6* is regulated by canonical Wnt signaling through *lef1* in the leading region of the pLLP and is required to inhibit Fgf activity (Matsuda et al., 2013). Whereas *dusp6* was expressed in the leading and mid-region in WT primordia (Fig. 4S,U,W), its expression was absent in the leading region of the *krm1*^{nl10} mutant at 32 hpf (Fig. 4T) and restricted to the mid-zone and last-deposited NMs at 36 and 40 hpf (Fig. 4V,X). However, expression of the Wnt target *fgf10a* (Aman and Piotrowski, 2008; Matsuda et al., 2013) and the Fgf target *pea3* were not grossly altered in *krm1*^{nl10} primordia

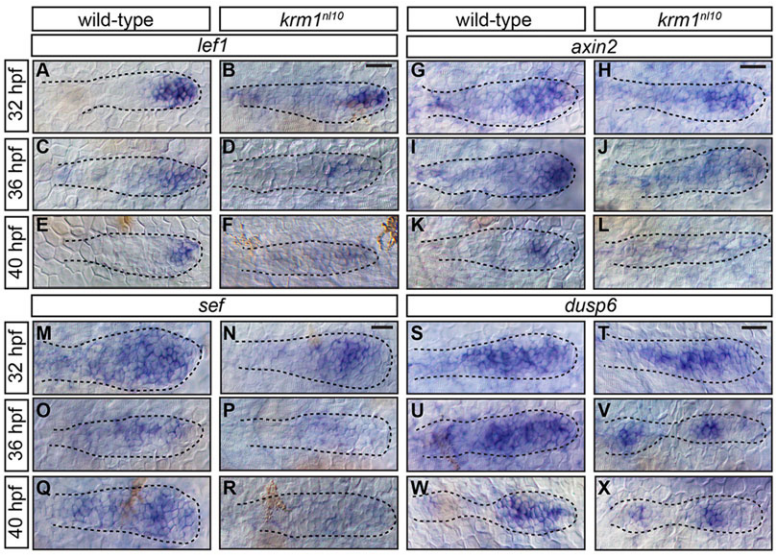

Fig. 4. Wnt activity is prematurely and progressively decreased in *krm1*^{nl10} mutants. (A-R) Expression of the Wnt targets, *lef1*, *axin2* and *sef*, in the pLLP at 32, 36 and 40 hpf in WT and *krm1*^{nl10} embryos. In WT primordia, expression domains of *lef1* (A,C,E), *axin2* (G,I,K) and *sef* (M,O,Q) are progressively decreased between 32 and 40 hpf. In *krm1*^{nl10} mutant primordia, Wnt target expression is similar to WT at 32 hpf (B,H,N). At 36 hpf, expression domains are decreased in mutants compared with WT (D,J,P), and are absent in mutants at 40 hpf (F,L,R). *dusp6* is expressed in the leading and mid-zones of WT primordia between 32 and 40 hpf (S,U,W); expression is absent in the leading zone of *krm1*^{nl10} mutant primordia at these stages (T,V,X). Scale bars: 20 µm.

Development (2014) 141, 3212-3221 doi:10.1242/dev.102541

Table 1. Analysis of *lef1* expression during pLLP migration

	32 hpf	36 hpf	40 hpf
WT	6/6 (100%)	12/14 (85.7%)	7/11 (77%)
krm1^{nl10}	6/8 (75%)	4/15 (26.7%)	5/20 (25%)

The number and percentage of WT or *krm1*^{nl10} mutant embryos with high levels of *lef1* expression in the pLLP at 32, 36 or 40 hpf.

(supplementary material Fig. S7A-L). Expression of the chemokines *cxcr4b* and *cxcr7b* that are required for proper pLLP migration were also not altered in *krm1*^{nl10} mutants compared with WT embryos (supplementary material Fig. S8A-D). Altogether, these data indicate that Wnt-mediated transcription is prematurely and progressively reduced, but not completely abolished in *krm1*^{nl10} primordia.

Loss of Kremen1 function leads to non-cell-autonomous defects in the pLLP

Because Kremen1 is a transmembrane receptor protein, we reasoned that decreased Wnt activity observed in *krm1*^{nl10} mutants might be rescued by introducing WT cells into *krm1*^{nl10} primordia. Mosaic WT embryos containing WT donor cells showed full extension of the pLL (6/6 embryos; Fig. 5A,B; supplementary material Fig. S9A,A′; Table 2). Surprisingly, presence of WT donor cells in *krm1*^{nl10} mutant pLLPs was unable to rescue pLL extension (0/16 embryos; Fig. 5C; supplementary material Fig. S9B,B′; Table 2). By contrast, similar numbers of WT donor cells were able to rescue pLL formation in *lef1*^{nl2} mutant hosts (5/5 embryos; supplementary material Fig. S9E,E′; Table 2) (McGraw et al., 2011). A similar non-cell-autonomous defect in pLLP migration was observed in mosaic embryos containing *Tg(hsp70l:dkk1b-GFP)* donor cells that were induced to secrete Dkk1b following heat shock (0/6 embryos showed tc formation; supplementary material Fig. S8D,D′; Table 2) (McGraw et al., 2011). Finally, mosaic embryos containing *krm1*^{nl10} donor cells on a WT background showed full pLL formation (10/10 embryos; supplementary material Fig. S9C,C′; Table 2). These results indicate that loss of Kremen1 function leads to non-cell-autonomous defects in mutant pLLP, similar to those induced by Dkk1b secretion; by contrast, mutant cells behave normally in a WT background.

The failure of WT donor cells to rescue the *krm1*^{nl10} phenotype could be explained by a non-cell-autonomous loss of Wnt signaling in these cells. We tested this by generating mosaic embryos that contained *Tg(7xtcf-siam:eGFP)* donor cells in WT or *krm1*^{nl10} hosts. At 24 hpf, GFP-positive donor cells were present in both WT and mutant host primordia (Fig. 5E,F,I). By 48 hpf, GFP-positive cells contributed to the deposited NMs, including the tc NMs of WT hosts (Fig. 5G,I; supplementary material Movie 3). By contrast, the majority of donor cells in *krm1*^{nl10} mutant hosts downregulated GFP and possibly underwent cell death, as indicated by the rhodamine-positive cell fragments in the pLLP (blue arrowheads; Fig. 5H,I; supplementary material Movie 4). Together, these data suggest that loss of Kremen1 function results in a non-cell-autonomous decrease in Wnt signaling in *krm1*^{nl10} primordia.

Attenuation of Dkk partially rescues the *krm1*^{nl10} phenotype

Based on our data, we hypothesized that a loss of Wnt signaling in *krm1*^{nl10} mutant pLLPs resulted from an expansion of Dkk activity. Unfortunately, we were unable to obtain commercial antibodies that recognized zebrafish Dkk1b or Dkk2 proteins to directly test this model. Thus, we used a number of approaches to decrease Dkk activity in WT and *krm1*^{nl10} embryos. We reasoned that if our hypothesis was correct, attenuating Dkk activity should rescue the pLL truncation in *krm1*^{nl10} mutants.

Fgf signaling in the pLLP is known to be required for the proper expression of *dkk1b* (Aman and Piotrowski, 2008). Thus, we decreased Dkk function in the pLLP by attenuating Fgf signaling with the pharmacological inhibitor SU5402 (Mohammadi et al., 1997). WT and *krm1*^{nl10} embryos were treated with a suboptimal dose of SU5402 (a dose that did not cause pLL patterning defect in WT) or DMSO (control) beginning at 24 hpf, and the extent of pLLP migration and NM spacing were analyzed at 2 dpf. As expected, *dkk1b* expression was decreased and *lef1* expression increased following SU5402 treatment in both WT and *krm1*^{nl10} embryos when

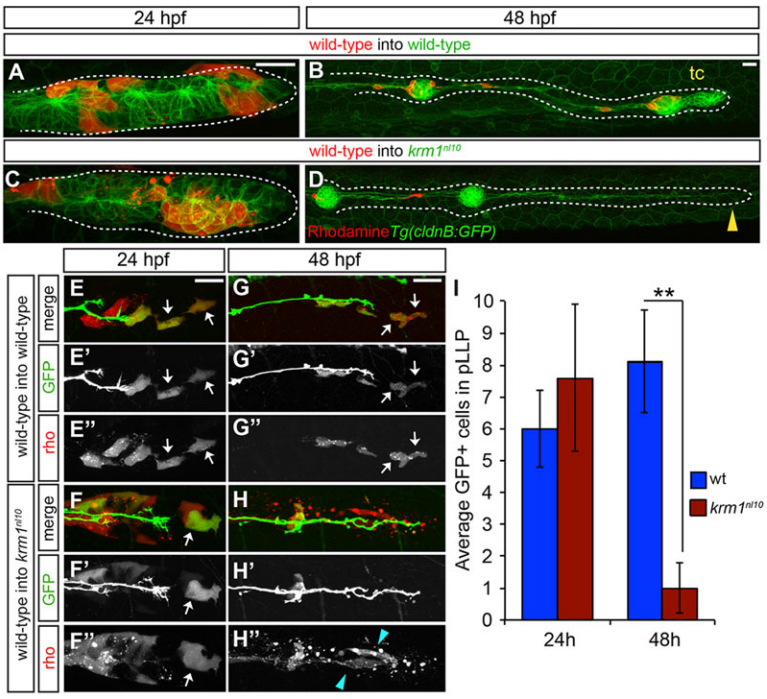

Fig. 5. Loss of Kremen1 leads to non-cell-autonomous defects in the pLLP. (A-D) Live confocal projections of mosaic, *Tg(cldnB:GFP)* WT or *krm1*^{nl10} embryos containing rhodamine-labeled donor cells (red) from WT donor embryos at 24 and 48 hpf. At 24 hpf, donor cells are found in the leading region of pLLP in WT (A) and mutant (C) hosts. At 48 hpf, the pLLP shown in A has migrated along the length of the trunk and formed the terminal cluster (tc; B), whereas the mutant pLLP in C has failed to migrate and diminished to a thin trail of cells (D, yellow arrowhead). (E-H″) Live confocal projections of WT and *krm1*^{nl10} host embryos that express *TgBAC(neuroD:eGFP)* and contain donor cells from *Tg(7xtcf-siam:eGFP)* donor embryos labeled with rhodamine (red). At 24 hpf, the leading region of primordia of both WT (E-E″) and mutant (F-F″) hosts contain GFP-positive (E′,F′) and rhodamine-positive (E″,F″) donor cells (white arrows). At 48 hpf, GFP/rhodamine-positive cells remain in the leading zone of WT primordia (G-H″, white arrows). In *krm1*^{nl10} mutant primordia, few GFP-positive cells remain (H-H′), and the remaining rhodamine-positive donor cells are fragmented and appear to undergo cell death (H″; blue arrowheads). (I) Quantification of *Tg(7xtcf-siam:eGFP)*-positive donor cells at 24 hpf and 48 hpf in control (WT donor cells in WT hosts) and experimental (WT donor cells in *krm1*^{nl10} hosts) primordia (n=5 *krm1*^{nl10} hosts, 10 WT hosts; $^{**}P$=0.007, Student's t-test). Scale bars: 20 µm.

Development (2014) 141, 3212-3221 doi:10.1242/dev.102541

Table 2. pLL formation in chimeric embryos

Donor	Host	Donor cells at 24 hpf	tc at 48 hpf
WT	WT	10.8 (±4.2)	6/6
WT	*krm1*^{nl10}	8.9 (±5.7)	0/16
krm1^{nl10}	WT	9.0 (±2.0)	10/10
hs:dkk1b	WT	11.3 (±4.4)	0/6
WT	*lef1*^{nl2}	9.8 (±2.7)	5/5

Mean (±s.d.) of donor cells in the leading region (first 30 cells) of host pLLPs at 24 hpf and presence of a terminal cluster (tc) at 48 hpf. There is no significant difference in the number of donor cells between conditions at 24 hpf (P=0.74, one-way ANOVA).

compared with DMSO-treated controls (Fig. 6G-N). We found that NM spacing, but not NM number, was rescued in the treated *krm1*^{nl10} mutant embryos, and that WT primordia migrated to the end of the tail to deposit a full complement of NMs (Fig. 6A-F). BrdU incorporation indicated that proliferation was not rescued in SU5402-treated *krm1*^{nl10} mutants compared with DMSO-treated controls and was decreased in SU5402 WT pLLP (supplementary material Fig. S10). These results suggest that reduction of Dkk levels through inhibition of Fgf signaling partially rescues pLLP patterning in *krm1*^{nl10} mutants.

Next, we blocked Dkk function by injecting WT or *krm1*^{nl10} zygotes with *dkk1b* and/or *dkk2* splice-blocking morpholinos (supplementary material Fig. S11A-C). In all conditions, including control embryos, *p53*-MO was also co-injected to minimize non-specific cell death. Injection of the individual *dkk*-MOs resulted in a small but significant increase in the number of deposited NMs in *krm1*^{nl10} mutants compared with *krm1*^{nl10} embryos injected with *p53*-MO (supplementary material Fig. S11D). Co-injection of both *dkk1b/2*-MOs resulted in a rescue of NM numbers comparable to that of WT (supplementary material Fig. S11D). WT embryos injected with *dkk1b*, *dkk2* or *dkk1b/2*-MOs did not show a significant change in NM number compared with WT p53 morphants, although their NMs were shifted caudally (supplementary material Fig. S11D; Fig. 7A,C,E). *krm1*^{nl10} embryos injected with *dkk1b/2*-MOs showed a partial rescue of NM spacing compared with control *krm1*^{nl10} embryos (Fig. 7B,D,E); in a subset of embryos, the pLLP migrated to the end of the tail. In addition, *krm1*^{nl10} embryos injected with *dkk1b/2*-MOs showed rescue of BrdU incorporation levels (Fig. 7J-N). Both WT and mutant embryos also showed expanded *lef1* expression domains in the primordia following *dkk1b/2*-MO injection (Fig. 7F-I). This is consistent with a previous report, indicating that the size of the Wnt signaling domain in the pLLP regulated NM spacing (Matsuda et al., 2013). Together, these results support the model that expansion of Dkk activity in *krm1*^{nl10} mutants is responsible for the premature loss of Wnt activity in the pLLP. When Dkk function is inhibited by *dkk1b/2*-MO injection, Wnt activity and cellular proliferation are restored in *krm1*^{nl10} mutants, which in turn results in partial to full rescue of NM number and spacing.

Kremen1 restricts the spread of Dkk1b protein in the pLLP

Based on our data, we predicted that Kremen1 acts to restrict the domain of Dkk activity in the pLLP. To examine the behavior of Dkk1b protein during pLLP migration, we generated a tagged version of Dkk1b under the control of the heat shock promoter (*hsp70:dkk1b-mTangerine*). Mosaic expression of the ectopic Dkk1b-mTangerine protein beginning at 25 hpf resulted in severe pLL truncation and loss of NMs in both WT and *krm1*^{nl10} embryos at 2 dpf (supplementary material Fig. S12). This phenotype is

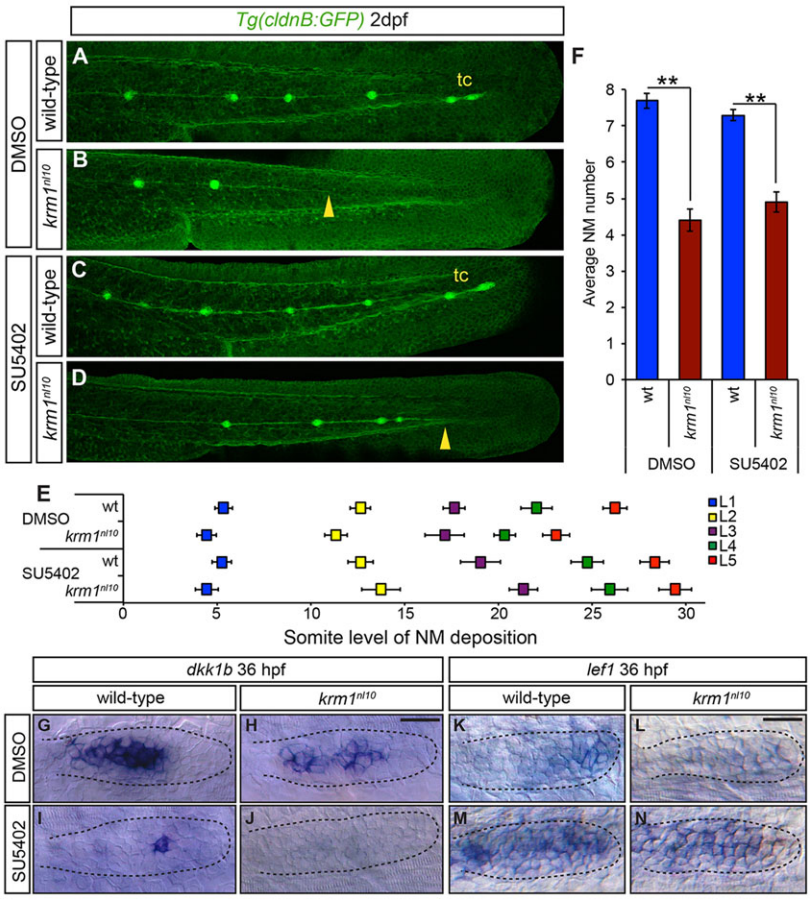

Fig. 6. Inhibition of Fgf signaling partially rescues NM spacing in *krm1*^{nl10} mutants. (A-D) Confocal projection of 2 dpf *Tg(cldnB:GFP)* WT or *krm1*^{nl10} embryos, treated with either DMSO (controls) or SU5402. (A,E) DMSO-treated WT embryos show full pLLP extension and tc formation. (B,E) *krm1*^{nl10} mutants treated with DMSO show pLL truncation midway along the trunk (yellow arrowhead). (C,E) Suboptimal SU5402 treatment of WT embryos results in normal pLL extension and tc formation. (D,E) In *krm1*^{nl10} mutants, pLLP migration is partially rescued and pLL is extended to the end of the tail (yellow arrowhead), although tc NMs are rarely present (n=10 embryos per condition; P<0.001, two-way ANOVA with replication). (F) NM numbers are not significantly different between WT embryos treated with DMSO or SU5402 and between *krm1*^{nl10} mutants treated with DMSO or SU5402 (n=10 embryos/condition; **P<0.001, Student's t-test). (G-N) Expression of *dkk1b* or *lef1* in WT and *krm1*^{nl10} pLLPs treated with DMSO or SU5402 at 36 hpf. *dkk1b* is expressed in the mid-region of the pLLP of DMSO-treated WT (G) and mutant (H) embryos. In SU5402-treated embryos, *dkk1b* expression is reduced in WT pLLP (I) and absent in *krm1*^{nl10} pLLP (J). *lef1* is expressed in the leading region of WT primordia (K) and absent in *krm1*^{nl10} mutant primordia treated with DMSO (L). SU5402 treatment results in increased *lef1* expression in WT (M) and mutant (N) primordia. Scale bars: 20 µm.

Development (2014) 141, 3212-3221 doi:10.1242/dev.102541

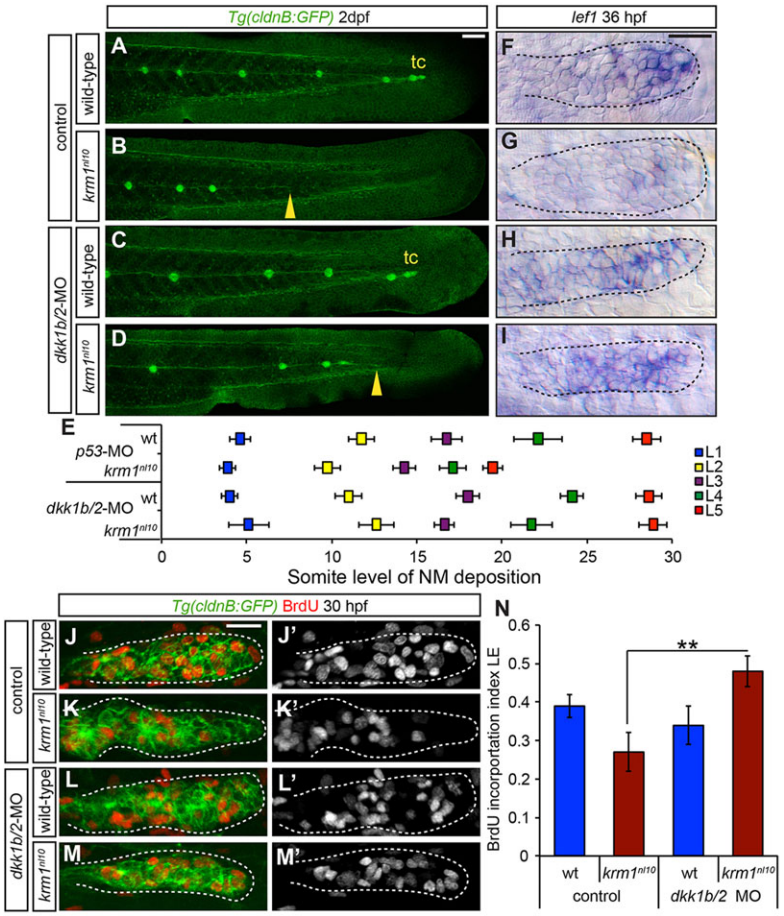

Fig. 7. *dkk1b/2* morpholino injections rescue *krm1*^{nl10} pLL formation. (A-D) Confocal projection of 2 dpf *Tg(cldnB:GFP)* WT or *krm1*^{nl10} embryos, injected with either control or *dkk1b/2*-MOs. (A) Control WT embryos show full pLLP migration and tc formation. (B) Control *krm1*^{nl10} embryos display characteristic premature stalling of the pLLP (yellow arrowhead). (C) Injection of *dkk1b/2*-MOs in WT embryos results in full pLLP migration and tc formation, although NM spacing is shifted posteriorly. (D) In *krm1*^{nl10} mutants injected with *dkk1b/2*-MOs, pLLP migration and pLL formation are partially rescued (yellow arrowhead). (E) NM spacing in *krm1*^{nl10} mutants injected with *dkk1b/2*-MOs is not significantly different from WT control NMs (*n*=8 embryos/condition; *P*<0.001, two-way ANOVA with replication). (F-I) *lef1* expression at 36 hpf is restricted to the pLLP leading region in control WT pLLP (F) and downregulated in control *krm1*^{nl10} mutant pLLP (G). *dkk1b/2*-MO injection results in an expansion of *lef1* expression in both WT (H) and *krm1*^{nl10} (I) primordia. (J-M′) Confocal projections of BrdU incorporation in both WT and *krm1*^{nl10} control and *dkk1b/2*-MO-injected embryos at 30 hpf. BrdU incorporation index is high in the leading region of control WT embryos (J,J′,N) and significantly decreased in *krm1*^{nl10} mutants (K,K′,N). *dkk1b/2*-MO injection results in no change in WT (L,L′,N) and in a significant increase in the BrdU incorporation index in the leading region of *krm1*^{nl10} mutant primordia (M,M′,N) (*n*=10 embryos per condition; ***P*=0.007, Student's *t*-test). Scale bars: 20 µm.

consistent with global induction of Dkk1b expression (McGraw et al., 2011) and indicates that the fusion protein is functional. To examine the behavior of tagged Dkk1b protein during pLLP migration, we heat-shocked injected embryos at 25 hpf and examined the spread of mTangerine fluorescence in WT and *krm1*^{nl10} embryos at 28 hpf, prior to the onset of Dkk1b-induced cell death. We only analyzed primordia containing between one and three Dkk1b-mTangerine-positive cells, so we could unambiguously determine the source of the secreted fusion protein. In mutant primordia, we found a significant increase in the amount of Dkk1b-mTangerine at two cell diameters from the expressing cell compared with WT primordia. Importantly, despite the transient nature of the transgene expression, there was no significant difference in mTangerine levels within the source cells (Fig. 8A-D). These data suggest that Kremen1 is necessary to limit the spread, and possibly the subsequent activity, of Dkk1b in the pLLP.

DISCUSSION

In this paper, we describe a novel zebrafish mutant strain (*krm1*^{nl10}) that carries a genetic lesion in *kremen1*, a non-obligate co-receptor for the Dkk family of secreted Wnt inhibitors. *krm1*^{nl10} mutants fail to form a complete pLL due to a loss of Wnt signaling in the leading region of the pLLP, which in turn results in a decreased cellular proliferation, increased cell death and loss of Wnt target gene expression. Transplantation of WT donor cells into the *krm1*^{nl10} primordia failed to rescue the mutant phenotype, demonstrating the non-cell-autonomous effects of the mutation. In mosaic embryos, *krm1*^{nl10} donor cells were able to contribute to pLL formation in a WT host, consistent with the role of Kremen1 as a non-obligate receptor for Dkk. Attenuation of Dkk levels either partially or completely rescued pLL formation in the *krm1*^{nl10} mutants. Our overexpression experiments also demonstrated that the Dkk1b fusion protein has a more extensive spread from the source cell in the mutant background. We conclude that Kremen1 restricts the domain of Dkk to the mid-region of the pLLP, probably through mediating the endocytosis of the Dkk-Lrp5/6 complex. In the absence of Kremen1 function, Dkk improperly spreads and inhibits normal Wnt signaling (supplementary material Fig. S13). This represents a previously unidentified mechanism for the precise modulation of canonical Wnt activity in the context of collective cell migration.

Kremen1 is required to modulate Wnt activity in the pLLP

Previous *in vitro* and *in vivo* studies have demonstrated that Kremen1 acts together with Dkk to inhibit Wnt signaling and that loss of Kremen1 results in overactivation of canonical Wnt signaling (Nakamura et al., 2008). By contrast, we observed phenotypes consistent with Wnt inhibition in the pLLP of the *krm1*^{nl10} mutants. The evidence for this included: truncation of the pLL and an anterior shift in the spacing of the deposited NMs; phenotypes observed during inhibition of Wnt signaling (McGraw et al., 2011; Valdivia et al., 2011; Matsuda et al., 2013); expression of Wnt target genes during pLLP migration were prematurely and progressively decreased in *krm1*^{nl10} mutants; expression of the Wnt sensor line *Tg(7xtcf-siam:eGFP)* was decreased in *kremen1* morphants; and absence of Wnt-dependent *dusp6* expression (Matsuda et al., 2013) in the leading region of *krm1*^{nl10} mutant primordia. Additionally, we observed a decrease

Development (2014) 141, 3212-3221 doi:10.1242/dev.102541

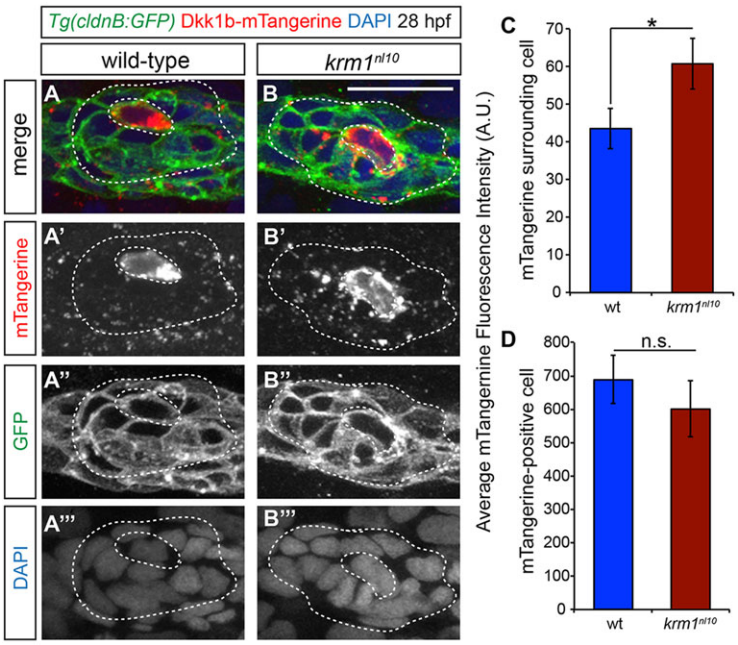

Fig. 8. Mosaic expression of *Dkk1b*-mTangerine shows a greater spread in *krm1*^{nl10} primordia. (A-B‴) Confocal projections of 28 hpf WT and *krm1*^{nl10} pLLP showing mosaic expression of Dkk1b-mTangerine driven by heat shock promoter, which was activated at 25 hpf. (A-A‴) WT showing expression of Dkk1b-mTangerine in a single cell (inner dashed lines) and low expression levels in surrounding cells (outer dashed lines). (B-B‴) *krm1*^{nl10} mutant expressing Dkk1b-mTangerine in a single cell (inner dashed lines) and punctate expression in surrounding cells (outer dashed lines). (C) Quantification of mTangerine fluorescence intensity in arbitrary units (A.U.). ROI: two cell diameters from the mTangerine-expressing source cell, excluding the source cell, minus background. (D) Quantification of mTangerine expression intensity in the source cell (A.U.) shows no significant difference between WT and mutant cells. Note that *krm1*^{nl10} mutants show a significant increase in fluorescence intensity compared with WT (n=31 WT and n=30 *krm1*^{nl10} primordia in six separate experiments; $^{**}P$<0.04, Student's t-test). Scale bar: 20 µm.

in BrdU incorporation and an increase in cell death in the pLLPs of *krm1*^{nl10} mutants. Lineage labeling of progenitor cells in the pLLP further revealed that cells in *krm1*^{nl10} mutants failed to divide and remained in the leading region. Altogether, *krm1*^{nl10} mutants displayed a gradual loss of Wnt activity that resembled the phenotype seen after ectopic activation of Dkk1b activity (Aman et al., 2011; McGraw et al., 2011).

Dkk activity is ectopically expanded following loss of Kremen1 function

Based on the loss of Wnt activity phenotype and additional experiments (mosaic analyses, attenuation of Dkk expression and analysis of tagged-Dkk1b protein), we propose a model in which Kremen1 plays a role in limiting the range of Dkk proteins in the pLLP. We propose that in *krm1*^{n10} mutants, the absence of Kremen1 results in a failure of Dkk-Lrp5/6 endocytosis, leading to the spread of Dkk throughout the pLLP and to improper diminishment of Wnt activity in the leading region. Generation of mosaic embryos containing WT donor cells in *krm1*^{nl10} mutant hosts revealed that the absence of Kremen1 function resulted in non-cell-autonomous defects, i.e. a failure by donor cells to rescue the *krm1*^{nl10} phenotype. Additional mosaic analyses using *Tg(7xtcf-siam:eGFP)* donor cells in *krm1*^{nl10} hosts showed a distinct non-cell-autonomous loss of Wnt-mediated GFP expression in transplanted cells. This result is strikingly different from that observed in mosaic *lef1*^{nl2} embryos containing WT donor cells, which showed complete rescue of the pLL (McGraw et al., 2011), again underscoring the non-cell-autonomous nature of the *krm1*^{nl10} mutant phenotype. How could mutation of Kremen1, a membrane-localized receptor, exert non-cell-autonomous defects on cells in the pLLP? As Kremen1 is a receptor for the secreted Wnt inhibitor Dkk and regulates endocytosis of the Kremen1-Dkk-Lrp5/6 complex (Mao et al., 2002), we reasoned that in *krm1*^{nl10} mutants, Dkk was perhaps not properly cleared from the pLLP. We were unable to directly test this model due to a lack of antibodies that recognize zebrafish Dkk proteins. Thus, we used indirect methods, such as attenuation or blocking of Dkk activity and ectopic expression of tagged Dkk1b protein. When we decreased Dkk levels in the mutant pLLPs either by blocking Fgf signaling, which regulates *dkk1b* expression in the pLLP (Aman and Piotrowski, 2008), or by *dkk1b/2* morpholino injections, we found a partial rescue pLL formation in *krm1*^{nl10} mutants. Mosaic expression of tagged Dkk1b protein in WT and *krm1*^{nl10} mutant primordia revealed a significant increase in the spread of Dkk1b-mTangerine in mutant pLLP. Together, these results support our model that Kremen1 functions to restrict the domain of Dkk activity in the pLLP. Future work is required to examine the behavior of native Dkk1b protein in these mutants.

Kremen1/2 can function to facilitate Wnt activity in the absence of Dkk

We show that *kremen1*, but not *dkk1b/2*, is expressed in the leading region of the pLLP. This raises the question of whether Kremen1 might have another function in addition to acting as a Dkk receptor. Previous work *in vitro* demonstrated that, in the absence of Dkk1, Kremen1/2 binds to and stabilizes Lrp6 at the cell surface, thus promoting Wnt activity. Additionally, Dkk2 has been shown to stimulate Wnt signaling during neural crest induction (Hassler et al., 2007). The possibility that Kremen1 might also play a role in promoting Wnt activity in the pLLP is compatible with our model, in which Kremen1 is also required to restrict the range of Dkk activity. However, inhibiting Dkk1b/2 function is able to partially or fully rescue pLL formation in *krm1*^{nl10} mutants, which argues against Kremen1 promoting Wnt activity. Future work is needed to determine whether Kremen1 has additional roles in modulating Wnt signaling in the pLLP.

In conclusion, we have shown that Kremen1 modulates Wnt signaling in the pLLP and is required for proper collective cell migration. Our data indicate that in the absence of Kremen1 function, Wnt signaling is prematurely downregulated in the pLLP in a non-cell-autonomous manner through an ectopic expansion of Dkk proteins. As improper Wnt signaling has been implicated in collective cancer invasion (Friedl and Gilmour, 2009), and expression of *kremen1* is altered in some cancers (Dun et al., 2010; Murphy et al., 2012), our findings may provide a potential mechanism for Wnt misregulation during disease.

Development (2014) 141, 3212-3221 doi:10.1242/dev.102541

MATERIALS AND METHODS

Zebrafish strains

Embryonic and adult zebrafish were staged and maintained according to standard protocols (Kimmel et al., 1995). The transgenic fish strains used were: *Tg(-8.0claudinB:lyneGFP)*^{zf106}, referred to as *Tg(cldnB:GFP)* (Haas and Gilmour, 2006), *Tg(neuroD:eGFP)*^{nl1} (Obholzer et al., 2008), *Tg(hsp70l:dkk1b-GFP)*^{w32} (Stoick-Cooper et al., 2007) and *Tg(7xtcf-siam:eGFP)*^{ia4} (Valdivia et al., 2011; Moro et al., 2012).

Positional cloning of *krm1*^{nl10} and mRNA injections

The genetic lesion underlying the *krm1*^{nl10} phenotype was identified using standard simple sequence length polymorphism (SSLP) mapping techniques (Gates et al., 1999). To identify polymorphisms, heterozygous carriers of *krm1*^{nl10} on a polymorphic *AB/WIK background were intercrossed to produce homozygous, heterozygous and WT progeny. The *krm1*^{nl10} lesion was located on the distal arm of chromosome 5, in the *kremen1* gene (GenBank accession number: BC158176.1). WT and mutant mRNAs were generated using the mMessage kit (Ambion) and were injected at 200 pg/nl into one-cell stage zygotes.

RNA *in situ* hybridization, immunolabeling, TUNEL labeling, BrdU-incorporation and DASPEI labeling

RNA *in situ* hybridization was performed using standard protocols (Andermann et al., 2002). Antisense RNA probes generated were: *lef1* (Dorsky et al., 1999), *axin2* (Aman and Piotrowski, 2008), *fgf10a* (Grandel et al., 2000), *pea3* (Raible and Brand, 2001; Roehl and Nüsslein-Volhard, 2001), *sef* (Aman and Piotrowski, 2008), *dusp6* (Lee et al., 2005), *dkk1b* (Aman and Piotrowski, 2008), *cxcr4b* and *cxcr7b* (Dambly-Chaudiere et al., 2007). We cloned full-length cDNA and used it to generated probes for *kremen1* (forward RT-PCR primer: AGTGTTATACAGCGAATGG, reverse RT-PCR primer: TTAGTTTCCCACAAGTGGG) and *dkk2* (forward RT-PCR primer: ATGCTCACTGTTACGAGGAGT, reverse RT-PCR primer: GTATGGATCGTCCCTTCTTAG). Whole-mount immunolabeling was performed following established protocols (Ungos et al., 2003). The following antibodies were used: rabbit or mouse anti-GFP (Life Technologies, A11122 and A11120, respectively; both 1:1000), rat anti-BrdU (Abcam, ab6326; 1:100), rabbit anti-activated caspase 3 (Cell Signaling, 9664; 1:200), Alexa 488 (Life Technologies, A11001; 1:1000) and Alexa 568 (Life Technologies, A11011; 1:1000). TUNEL labeling was performed using an established protocol modified for fluorescent detection (Nechiporuk et al., 2005). BrdU incorporation was carried out using established protocols (Harris et al., 2003; Laguerre et al., 2005). Adult NMs were labeled with 0.005% 2-[4-(dimethylamino) styryl]-N-ethylpyridinium iodide (DASPEI; Life Technologies) in embryo medium for 20 min at room temperature.

Imaging, Kaede photoconversion and time-lapse microscopy

Confocal analyses and time-lapse imaging were performed using an Olympus FV1000 confocal system. Nomarski images were collected using a Zeiss Imager Z1 compound microscope. Individual cells were lineage-labeled using photoconversion of the Kaede fluorophore as previously described (Ando et al., 2002; McGraw et al., 2011). Cell counts were determined using DAPI (30 µM; Life Technologies)-labeled nuclei. For time-lapse imaging, embryos were analyzed between 36 and 48 hpf using established techniques (McGraw et al., 2011). Images were processed using ImageJ software (Abramoff et al., 2004). Brightness and contrast were adjusted using the Adobe Photoshop software package.

Morpholino injections and inhibitor treatment

All antisense oligonucleotide morpholinos (Genetools) were co-injected with the p53-MO (Robu et al., 2007) at twice the concentration of the experimental MOs. The p53-MO was injected at 10 µg/µl for control experiments. A translation-blocking MO against *kremen1* (a gift from the Weinstein laboratory, 5′-AAGCTGCGACTCTCCACGAATCCAT-3′) (Gore et al., 2011) was injected at 0.5 µg/µl. Splice donor site-blocking MOs were designed against *dkk1b* exon 1/intron1 (*dkk1b*-MO: GCATATTTCTATGCTTACCTGCGGT) and *dkk2* exon2/intron2 (*dkk2*-MO: AATTGAACAAGCGTACAGTTGCTGC), and injected at 7 µg/µl. RT-PCR was carried out using *dkk1b*-forward ATGATGCACA-TCGCCATGCTC/*dkk1b*-reverse GCACACATGCCAGAGACACTAA and the *dkk2* primers described above. Fgf was inhibited using 75 µM SU5402 (Calbiochem) in embryo medium, and control embryos were treated with DMSO.

hsp70:dkk1b-mTangerine plasmid construction, injection and heat shock conditions

Full-length *dkk1b* was amplified by PCR from an EST clone (accession#: DV598280) using primers that contained *attB1* and *attB2* sites. Following amplification, PCR products were recombined into a pDONR221 vector, and the *hsp70:dkk1b-mTangerine* plasmid was assembled using components of the Tol2kit (Kwan et al., 2007). Ten pg/nl of the plasmid DNA was injected into one-cell stage embryos. At 25 hpf, embryos were heat-shocked at 39°C for 40 min using a thermocycler (Applied Biosystems).

Transplantation experiments

Transplantation experiments were carried out as previously described (Nechiporuk and Raible, 2008). In brief, rhodamine dextran (Life Technologies)-labeled donor cells from blastula stage embryos were transplanted in the left side of gastrula-stage host embryos. Host embryos were imaged at 24 hpf to determine the position of donor cells in the pLLP and at 48 hpf to assess pLL formation.

Data analysis and statistics

All data are presented as average±s.e.m. Fluorescence intensity was determined using the ImageJ analysis tool, and values (in arbitrary units, A.U.) were generated by selecting a region of interest (ROI) in the pLLP, collecting mean fluorescence intensity and then subtracting nearby background. For analysis of Dkk1b-mTangerine expression, the ROI was set at two cell diameters (based on DAPI and membrane marker expression) surrounding the Dkk1b-mTangerine-expressing cell, excluding the expressing cell itself. Separate expression levels were collected for the Dkk1b-mTangerine-expressing cell. Calculation of statistical significance was carried out using VassarStats (http://vassarstats.net/index.html).

Acknowledgements

We thank the Weinstein laboratory at The National Institute of Child Health and Human Development for reagents and David Kimelman and Catherine Drerup for comments on the manuscript.

Competing interests

The authors declare no competing financial interests.

Author contributions

H.F.M. conceived experiments, performed experiments, interpreted data and wrote the manuscript. M.D.C. performed experiments and A.V.N. conceived experiments and edited the manuscript.

Funding

This work was funded by The American Heart Association Postdoctoral Fellowship [11POST7210061] and The Collins Medical Trust Award to H.F.M. and by funds from the National Institute of Child Health and Human Development [1R01HD072844] and the American Cancer Society [RSG DDC-24733] to A.V.N. Deposited in PMC for release after 12 months.

Supplementary material

Supplementary material available online at
http://dev.biologists.org/lookup/suppl/doi:10.1242/dev.102541/-/DC1

References

Abramoff, M. D., Magelhaes, P. J. and Ram, S. J. (2004). Image processing with ImageJ. *Biophoton. Int.* **11**, 36-42.

Aman, A. and Piotrowski, T. (2008). Wnt/beta-catenin and Fgf signaling control collective cell migration by restricting chemokine receptor expression. *Dev. Cell* **15**, 749-761.

Aman, A. and Piotrowski, T. (2009). Multiple signaling interactions coordinate collective cell migration of the posterior lateral line primordium. *Cell Adh. Migr.* **3**, 365-368.

Aman, A., Nguyen, M. and Piotrowski, T. (2011). Wnt/β-catenin dependent cell proliferation underlies segmented lateral line morphogenesis. *Dev. Biol.* **349**, 470-482.
Andermann, P., Ungos, J. and Raible, D. W. (2002). Neurogenin1 defines zebrafish cranial sensory ganglia precursors. *Dev. Biol.* **251**, 45-58.
Ando, R., Hama, H., Yamamoto-Hino, M., Mizuno, H. and Miyawaki, A. (2002). An optical marker based on the UV-induced green-to-red photoconversion of a fluorescent protein. *Proc. Natl. Acad. Sci. USA* **99**, 12651-12656.
Chitnis, A. B., Nogare, D. D. and Matsuda, M. (2012). Building the posterior lateral line system in zebrafish. *Dev. Neurobiol.* **72**, 234-255.
Cselenyi, C. S. and Lee, E. (2008). Context-dependent activation or inhibition of Wnt-beta-catenin signaling by Kremen. *Sci. Signal.* **1**, e10.
Dambly-Chaudière, C., Cubedo, N. and Ghysen, A. (2007). Control of cell migration in the development of the posterior lateral line: antagonistic interactions between the chemokine receptors CXCR4 and CXCR7/RDC1. *BMC Dev. Biol.* **7**, 23.
Davidson, G., Mao, B., del Barco Barrantes, I. and Niehrs, C. (2002). Kremen proteins interact with Dickkopf1 to regulate anteroposterior CNS patterning. *Development* **129**, 5587-5596.
Dorsky, R. I., Snyder, A., Cretekos, C. J., Grunwald, D. J., Geisler, R., Haffter, P., Moon, R. T. and Raible, D. W. (1999). Maternal and embryonic expression of zebrafish lef1. *Mech. Dev.* **86**, 147-150.
Dun, X., Jiang, H., Zou, J., Shi, J., Zhou, L., Zhu, R. and Hou, J. (2010). Differential expression of DKK-1 binding receptors on stromal cells and myeloma cells results in their distinct response to secreted DKK-1 in myeloma. *Mol. Cancer* **9**, 247.
Ellwanger, K., Saito, H., Clement-Lacroix, P., Maltry, N., Niedermeyer, J., Lee, W. K., Baron, R., Rawadi, G., Westphal, H. and Niehrs, C. (2008). Targeted disruption of the Wnt regulator Kremen induces limb defects and high bone density. *Mol. Cell. Biol.* **28**, 4875-4882.
Friedl, P. and Gilmour, D. (2009). Collective cell migration in morphogenesis, regeneration and cancer. *Nat. Rev. Mol. Cell Biol.* **10**, 445-457.
Gates, M. A., Kim, L., Egan, E. S., Cardozo, T., Sirotkin, H. I., Dougan, S. T., Lashkari, D., Abagyan, R., Schier, A. F. and Talbot, W. S. (1999). A genetic linkage map for zebrafish: comparative analysis and localization of genes and expressed sequences. *Genome Res.* **9**, 334-347.
Gore, A. V., Swift, M. R., Cha, Y. R., Lo, B., McKinney, M. C., Li, W., Castranova, D., Davis, A., Mukouyama, Y.-S. and Weinstein, B. M. (2011). Rspo1/Wnt signaling promotes angiogenesis via Vegfc/Vegfr3. *Development* **138**, 4875-4886.
Grandel, H., Draper, B. W. and Schulte-Merker, S. (2000). dackel acts in the ectoderm of the zebrafish pectoral fin bud to maintain AER signaling. *Development* **127**, 4169-4178.
Grigoryan, T., Wend, P., Klaus, A. and Birchmeier, W. (2008). Deciphering the function of canonical Wnt signals in development and disease: conditional loss- and gain-of-function mutations of beta-catenin in mice. *Genes Dev.* **22**, 2308-2341.
Haas, P. and Gilmour, D. (2006). Chemokine signaling mediates self-organizing tissue migration in the zebrafish lateral line. *Dev. Cell* **10**, 673-680.
Harding, M. J. and Nechiporuk, A. V. (2012). Fgfr-Ras-MAPK signaling is required for apical constriction via apical positioning of Rho-associated kinase during mechanosensory organ formation. *Development* **139**, 3130-3135.
Harris, J. A., Cheng, A. G., Cunningham, L. L., MacDonald, G., Raible, D. W. and Rubel, E. W. (2003). Neomycin-induced hair cell death and rapid regeneration in the lateral line of zebrafish (Danio rerio). *J. Assoc. Res. Otolaryngol.* **4**, 219-234.
Hassler, C., Cruciat, C.-M., Huang, Y.-L., Kuriyama, S., Mayor, R. and Niehrs, C. (2007). Kremen is required for neural crest induction in Xenopus and promotes LRP6-mediated Wnt signaling. *Development* **134**, 4255-4263.
Kimmel, C. B., Ballard, W. W., Kimmel, S. R., Ullmann, B. and Schilling, T. F. (1995). Stages of embryonic development of the zebrafish. *Dev. Dyn.* **203**, 253-310.
Kwan, K. M., Fujimoto, E., Grabher, C., Mangum, B. D., Hardy, M. E., Campbell, D. S., Parant, J. M., Yost, H. J., Kanki, J. P. and Chien, C.-B. (2007). The Tol2kit: a multisite gateway-based construction kit for Tol2 transposon transgenesis constructs. *Dev. Dyn.* **236**, 3088-3099.
Laguerre, L., Soubiran, F., Ghysen, A., König, N. and Dambly-Chaudière, C. (2005). Cell proliferation in the developing lateral line system of zebrafish embryos. *Dev. Dyn.* **233**, 466-472.
Lee, Y., Grill, S., Sanchez, A., Murphy-Ryan, M. and Poss, K. D. (2005). Fgf signaling instructs position-dependent growth rate during zebrafish fin regeneration. *Development* **132**, 5173-5183.
Lu, H., Ma, J., Yang, Y., Shi, W. and Luo, L. (2013). EpCAM is an endoderm-specific Wnt derepressor that licenses hepatic development. *Dev. Cell* **24**, 543-553.
Mao, B., Wu, W., Davidson, G., Marhold, J., Li, M., Mechler, B. M., Delius, H., Hoppe, D., Stannek, P., Walter, C. et al. (2002). Kremen proteins are Dickkopf receptors that regulate Wnt/beta-catenin signalling. *Nature* **417**, 664-667.
Matsuda, M., Nogare, D. D., Somers, K., Martin, K., Wang, C. and Chitnis, A. B. (2013). Lef1 regulates Dusp6 to influence neuromast formation and spacing in the zebrafish posterior lateral line primordium. *Development* **140**, 2387-2397.
McGraw, H. F., Drerup, C. M., Culbertson, M. D., Linbo, T., Raible, D. W. and Nechiporuk, A. V. (2011). Lef1 is required for progenitor cell identity in the zebrafish lateral line primordium. *Development* **138**, 3921-3930.
Mohammadi, M., McMahon, G., Sun, L., Tang, C., Hirth, P., Yeh, B. K., Hubbard, S. R. and Schlessinger, J. (1997). Structures of the tyrosine kinase domain of fibroblast growth factor receptor in complex with inhibitors. *Science* **276**, 955-960.
Moro, E., Ozhan-Kizil, G., Mongera, A., Beis, D., Wierzbicki, C., Young, R. M., Bournele, D., Domenichini, A., Valdivia, L. E., Lum, L. et al. (2012). In vivo Wnt signaling tracing through a transgenic biosensor fish reveals novel activity domains. *Dev. Biol.* **366**, 327-340.
Murphy, A. J., de Caestecker, C., Pierce, J., Boyle, S. C., Ayers, G. D., Zhao, Z., Libes, J. M., Correa, H., Walter, T., Huppert, S. S. et al. (2012). CITED1 expression in liver development and hepatoblastoma. *Neoplasia* **14**, 1153-1163.
Nakamura, T., Nakamura, T. and Matsumoto, K. (2008). The functions and possible significance of Kremen as the gatekeeper of Wnt signalling in development and pathology. *J. Cell. Mol. Med.* **12**, 391-408.
Nechiporuk, A. and Raible, D. W. (2008). FGF-dependent mechanosensory organ patterning in zebrafish. *Science* **320**, 1774-1777.
Nechiporuk, A., Linbo, T. and Raible, D. W. (2005). Endoderm-derived Fgf3 is necessary and sufficient for inducing neurogenesis in the epibranchial placodes in zebrafish. *Development* **132**, 3717-3730.
Obholzer, N., Wolfson, S., Trapani, J. G., Mo, W., Nechiporuk, A., Busch-Nentwich, E., Seiler, C., Sidi, S., Sollner, C., Duncan, R. N. et al. (2008). Vesicular glutamate transporter 3 is required for synaptic transmission in zebrafish hair cells. *J. Neurosci.* **28**, 2110-2118.
Osada, M., Ito, E., Fermin, H. A., Vazquez-Cintron, E., Venkatesh, T., Friedel, R. H. and Pezzano, M. (2006). The Wnt signaling antagonist Kremen1 is required for development of thymic architecture. *Clin. Dev. Immunol.* **13**, 299-319.
Raible, F. and Brand, M. (2001). Tight transcriptional control of the ETS domain factors Erm and Pea3 by Fgf signaling during early zebrafish development. *Mech. Dev.* **107**, 105-117.
Robu, M. E., Larson, J. D., Nasevicius, A., Beiraghi, S., Brenner, C., Farber, S. A. and Ekker, S. C. (2007). p53 activation by knockdown technologies. *PLoS Genet.* **3**, e78.
Roehl, H. and Nüsslein-Volhard, C. (2001). Zebrafish pea3 and erm are general targets of FGF8 signaling. *Curr. Biol.* **11**, 503-507.
Stoick-Cooper, C. L., Weidinger, G., Riehle, K. J., Hubbert, C., Major, M. B., Fausto, N. and Moon, R. T. (2007). Distinct Wnt signaling pathways have opposing roles in appendage regeneration. *Development* **134**, 479-489.
Ungos, J. M., Karlstrom, R. O. and Raible, D. W. (2003). Hedgehog signaling is directly required for the development of zebrafish dorsal root ganglia neurons. *Development* **130**, 5351-5362.
Valdivia, L. E., Young, R. M., Hawkins, T. A., Stickney, H. L., Cavodeassi, F., Schwarz, Q., Pullin, L. M., Villegas, R., Moro, E., Argenton, F. et al. (2011). Lef1-dependent Wnt/beta-catenin signalling drives the proliferative engine that maintains tissue homeostasis during lateral line development. *Development* **138**, 3931-3941.
Wada, H., Ghysen, A., Asakawa, K., Abe, G., Ishitani, T. and Kawakami, K. (2013). Wnt/Dkk negative feedback regulates sensory organ size in zebrafish. *Curr. Biol.* **23**, 1559-1565.

Supplementary Material Figure legends

Figure S1. The pLL is truncated in *krm1*^{nl10} adults

(**A,B**) DASPEI labeling of 4 months post fertilization (mpf) *Tg(cldnB:GFP)* expressing wild-type and *krm1*^{nl10} mutant adults. (**A**) A wild-type adult (24 mm in length) with DAPSEI labeled NMs on the trunk (blue arrows) and tail (blue brackets). (**B**) A 21 mm *krm1*^{nl10} mutant adult lacks the posterior-most trunk NMs (blue arrows) and all tail NMs.

Figure S2. The *krm1*^{nl10} mutation results in multiple cDNA splice variants

(**A**) Genomic DNA sequence for *kremen1* from wild-type and *krm1*^{nl10} mutant embryos showing the single base pair mutation from thymine (T) to cytosine (C; red asterisk) in the exon 6 splice donor site (black bar). (**B**) Schematic showing exons of wild-type *krm1*; the *krm1*^{nl10} lesion is located between exons 6 and 7 (red arrow). (**C**) Schematic representation of variant cDNAs generated from *krm1*^{nl10} embryos. (**D**) RT-PCR showing a single *krm1* cDNA band from wild-type embryos and multiple cDNA products from *krm1*^{nl10} embryos (see *krm1* primers in Materials and Methods). (**E**) Schematic showing wild-type Krm1 protein, including the signal peptide (SP), Kringle domain, WSC domain, CUB domain, Transmembrane domain and a short intracellular domain. Predicted protein variants from resulting from cryptic splicing of *krm1*^{nl10} . All schematics are not drawn to scale. (**F**) Quantification of *krm1* mRNA rescue following injection of

krm1 mRNA into embryos derived from *krm1*^{nl10}/+ X *krm1*^{nl10}/+ crosses. Injection of 200 pg/nl of *krm1* mRNA significantly increased the percentage of embryos that formed tc NMs (76% in uninjected and 98% in *krm1* mRNA injected), but did not affect NM number in wild-type embryos (n=51-58 embryos per condition; ***p*<0.001, *z*-test). In contrast injection of *krm1*^{nl10} V1 or V2 isoforms did not rescue NM number (74% in V1 injected and 76% in V2 injected embryos, n=36-49 embryos per condition).

Figure S3. Expression of *krm1, dkk1b* and *dkk2* partially overlaps throughout the embryo

(**A-B**) Expression domains of *krm1* and its ligands *dkk1b* and *dkk2* in 30 hpf wild-type embryos. (A) *krm1* is expressed in the mid-hindbrain boundary (mhb), lens (le), otic vesicle (ov), posterior lateral line primordium (pLLP) and the fin fold (ff). (**B**) *dkk1b* is expressed in the le, ov, pLLP and ff. (**C**) *dkk2* is expressed in the mhb, le, ov and pLLP.

Figure S4. The Wnt receptors *lrp5* and *lrp6* are expressed in the pLLP

(**A-B**) Expression of *lrp5* (**A**) and *lrp6* (**B**) throughout the primordia at 36 hpf in wild-type embryos. Scale bars=20 μm.

Figure S5. Cell death is increased in *krm1*^{nl10} mutant primordia

(A-B’’’) Confocal projections of 40 hpf wild-type (**A-A’’’**) and *krm1*^{nl10} (**B-B’’’**) labeled with activated Caspase3 antibody. Scale bars=20 µm. (n=35 embryos per condition, **p*<0.01, Fisher’s Exact Test).

Figure S6. Wnt activity is decreased following Krm1 knockdown.

(**A-D’’’**) Confocal projections of wild-type and *kremen1* morphant embryos expressing the Wnt sensor *Tg(7xtcf-siam:eGFP)* (green); nuclei are labeled with DAPI (blue). (**A-A’’, C-C’’**) GFP is expressed in cells of the leading part of a wild-type pLLP at 36 and 40 hpf. (**B-B’’,D-D’’**) In *kremen1*-MO injected embryos, GFP-positive cells are located throughout the pLLP, most are incorporated into proto-NMs (yellow arrows) and notably reduced in the leading region. By 40 hpf, the index of GFP-positive cells is significantly reduced in *kremen1* morphants (**E**). (**F**) The index of GFP in the leading zone of the pLLP (the caudal-most 30 cells of the pLLP) is significantly reduced in *kremen1* morphants at 36 and 40 hpf as compared to wild-type controls (n=10-12 embryos/condition; ***p*<0.001 Student’s *t*-test). Scale bars=20µm. (**G**) The mean fluorescence intensity of GFP-positive cells, measured in arbitrary units (A.U.), was significantly reduced in morphant primordia at both 36 and 40 hpf (n=10-12 embryos/condition; ***p*<0.001 Student’s *t*-test).

Figure S7. Members of the Fgf pathway are expressed in wild-type and *krm1*^{nl10} primordia

(**A-F**) Expression of *fgf10a* in wild-type and *krm1*^{nl10} primordia between 32 and 40 hpf. In wild-type embryos, *fgf10a* is expressed in the leading region of the primordia at 32, 36 and 40 hpf (**A,C,E**). A similar expression pattern for *fgf10a* was seen in *krm1*^{nl10} primordia (**B,D,F**). (**G-L**) Expression of the Fgf target *pea3* between 32 and 40 hpf. In wild-type (**G,I,K**) and *krm1*^{nl10} (**H,J,L**) embryos, expression of *pea3* is seen in the mid-zone of the primordia. Scale bars=20 µm.

Figure S8. Expression domains of chemokine receptors are not altered in *krm1*^{nl10} mutants

(**A-D**) Expression of *cxcr4b* and *cxcr7b* at 36 hpf in the primordia of wild-type and *krm1*^{nl10} mutants. *cxcr4b* is expressed in the leading and mid-zones of wild-type (**A**) and *krm1*^{nl10} (**B**) primordia. *cxcr7b* is expressed in the trailing zone of the wild-type (**C**) and mutant (**D**) primordia. Scale bars=20 µm.

Figure S9. pLL formation in mosaic embryos that contain *krm1*^{nl10}, *Tg(hsp701:dkk1b-GFP)* and *lef1*^{nl2} cells

(**A-E'**) Confocal projections of chimeric embryos with rhodamine-labeled donor cells (red) in *Tg(cldnB:GFP)*-positive hosts. At 24 hpf, donor cells are present in the leading region of primordia in wild-type to wild-type chimeras (**A**), wild-type to *krm1*^{nl10} (**B**), *krm1*^{nl10} to wild-type (**C**), *Tg(hsp701:dkk1b-GFP)* to wild-type (**D**) and wild-type to *lef1*^{nl2} mutants (**E**). At 2 dpf, pLL extension and terminal cluster (tc) formation was seen in wild-type to wild-type (**A'**), *krm1*^{nl10} to wild-type (**C'**)

and wild-type to *lef1*^{nl2} (**E'**). pLL formation was truncated in wild-type to *krm1*^{nl10} (**B'**) and *Tg(hsp701:dkk1b-GFP)* to wild-type (**D'**) chimeras. Scale bars=20 µm.

Figure S10. Cellular proliferation is not rescued by treatment with SU5402

(**A-D'**) Confocal projections of BrdU incorporation (red) in wild-type and *krm1*^{n10} embryos treated with DMSO or SU5402 between 24 and 34 hpf. BrdU label is present in the leading pLLP cells in DMSO treated wild-type (A-A'), but not mutant embryos (**C-C'**). SU5402 treatment resulted in reduced leading region BrdU incorporation in wild-type embryos (**B-B'**), but incorporation was not altered in SU5402 treated *krm1*^{nl10} mutants (**D-D'**). Scale bars=20 µm. (**E**) Quantification of the index of total BrdU incorporation in the pLLP showing no significant change in control versus treated wild-type embryos or control versus treated *krm1*^{nl10} mutants (n=11 embryos per condition, Student's *t*-test). (**E**) Quantification of the index of BrdU incorporation in the leading region of the pLLP shows a significant decrease in SU5402 treated wild-type embryos, but no change in *krm1*^{nl10} mutants (n=11 embryos per condition, Student's *t*-test).

Figure S11. Morpholino knockdown of Dkk1b and Dkk2 rescues NM number in *krm1*^{n10} mutants

(**A-C**) Injections of splice-blocking morpholinos against *dkk1b* (*dkk1b*-MO) and *dkk2* (*dkk2*-MO) result in improperly spliced RT-PCR products. (**A**) Schematic of the *dkk1b* gene, showing the location of RT-PCR primers (see Material and Methods; black arrows; 1b F/1b R). The *dkk1b*-MO blocks a splice donor site for

exon 1/intron 1. (**B**) Schematic of *dkk2* gene showing the location of RT-PCR primers (see Material and Methods; black arrows; 2 F/2 R). The *dkk2*-MO blocks the splice donor site for exon 2/intron 2. (**C**) RT-PCR using cDNA generated from uninjected or morphant embryos. Injection of *dkk1b*-MO or *dkk2*-MO results in misspliced transcripts. (**D**) Injections of *dkk1b*-MO, *dkk2*-MO or *dkk1b/2*-MOs did not alter the number of NMs deposited in wild-type embryos as compared to *p53*-MO injected controls. NM number was significantly increased in *krm1*^{nl10} mutants injected with *dkk1b*-MO, *dkk2*-MO or *dkk1b/2*-MOs as compared to *p53*-MO injected controls. (n=8 embryos per condition; $p>0.001$, one-way ANOVA). (**E**) NM spacing in wild-type embryo was not significantly altered by injection of *p53*-MO, nor were *krm1*^{nl10} mutants injected with *p53*-MO significantly different from uninjected controls NMs (n=10 embryos per condition, two-way ANOVA with replication).

Figure S12. Ectopic expression of Dkk1b-mTangerine results in decreased NM number and pLL truncation

(**A-D**) Confocal projections of 2 dpf embryos with ectopic expression Dkk1b-mTangerine (red) driven by heat-shock at 25 hpf. (**A**) Uninjected wild-type embryo show full pLL extension and terminal cluster (tc) formation, while uninjected *krm1*^{nl10} mutants show pLL truncation (**B**; yellow arrowhead). Dkk1b-mTangerine expression results in truncated pLL extension in both wild-type (**C**; yellow arrowhead) and *krm1*^{nl10} (**D**; yellow arrowhead) embryos. Scale bars=20 µm. (**E**) Quantification of NM number at 2 dpf; there is a significant decrease in

NM between uninjected control embryos (wild-type and *krm1*^{nl10} mutants) and embryos expressing Dkk1b-mTangerine (n=15, ***p*<0.001, two-way ANOVA with replication). There was no difference in NM number between wild-type and mutants expressing Dkk1b-mTangerine (n=15; Tukey's Post-Hoc Test).

Figure S13. Schematic model of Kremen1 activity in the pLLP

(**A**) In the wild-type pLLP, Kremen1 is expressed in the leading and mid-region of the pLLP. Dkk1b and Dkk2 are expressed in the mid-and trailing regions of the pLLP and are excluded from the leading region. Wnt signaling is active in the leading region and absent in the mid-and trailing regions, where Fgf signaling is active. (**B**) The *krm1*^{nl10} mutant pLLP lacks Kremen1 function, allowing for the spread of Dkk and inhibition of Wnt signaling in the leading region, resulting in truncated of pLL formation.

Figure S1

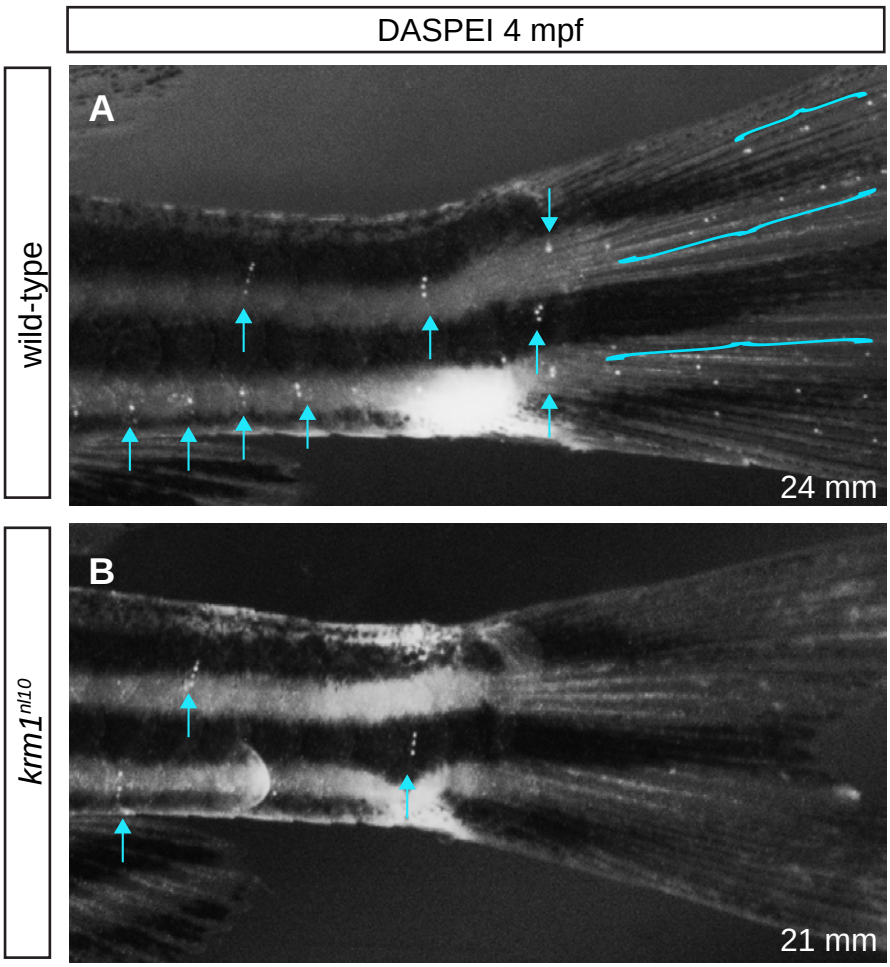

Figure S2

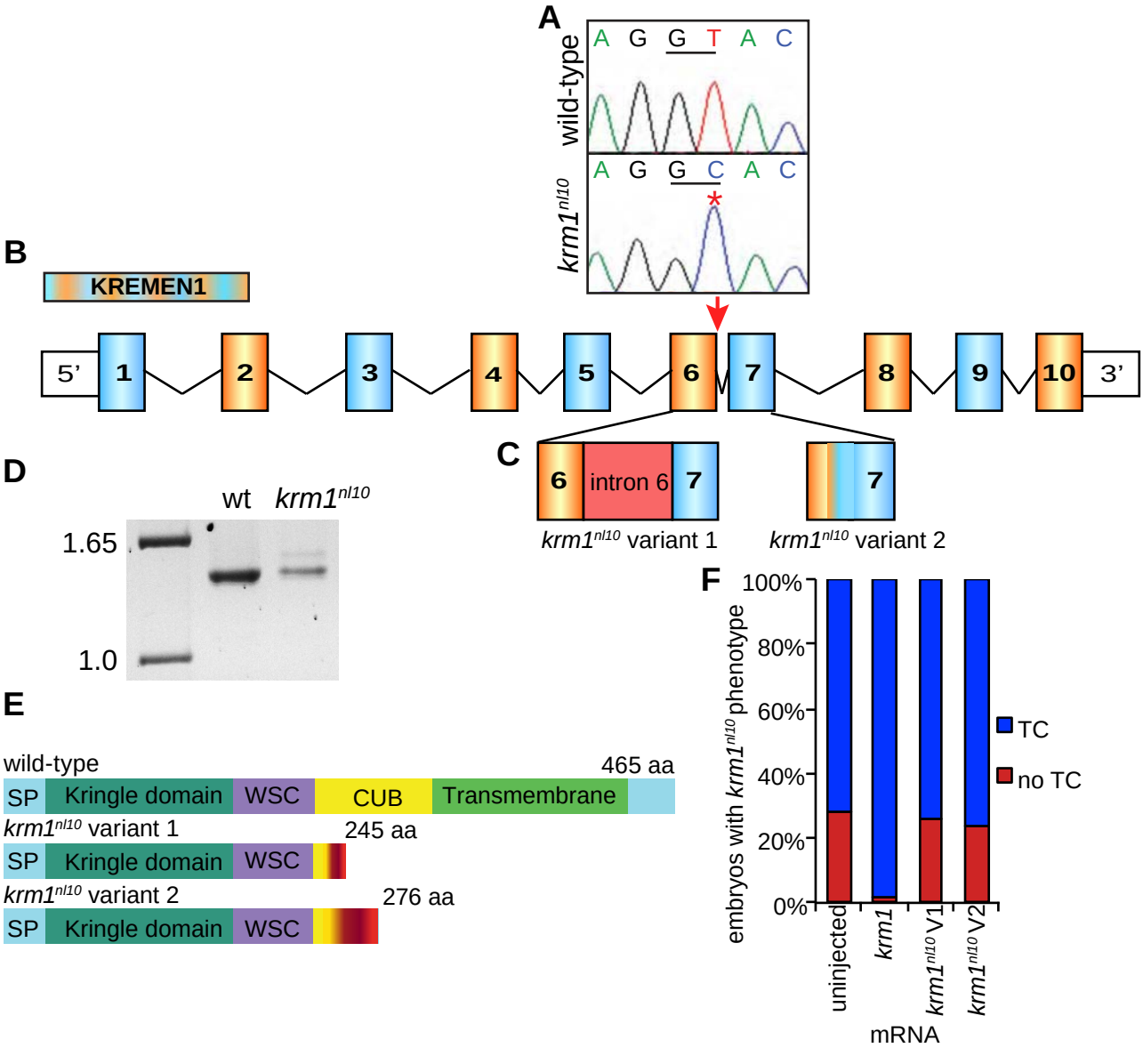
A
wild-type
A G G T A C
krm1nl10
A G G C A C
*
B
KREMEN1
5'
1
2
3
4
5
6
7
8
9
10
3'
C
6
intron 6
7
krm1nl10 variant 1
7
krm1nl10 variant 2
D
wt
krm1nl10
1.65
1.0
E
wild-type
465 aa
SP
Kringle domain
WSC
CUB
Transmembrane
krm1nl10 variant 1
245 aa
SP
Kringle domain
WSC
krm1nl10 variant 2
276 aa
SP
Kringle domain
WSC
F
embryos with krm1nl10 phenotype
100%
80%
60%
40%
20%
0%
TC
no TC
uninjected
krm1
krm1nl10V1
krm1nl10V2
mRNA

Figure S3

krm1

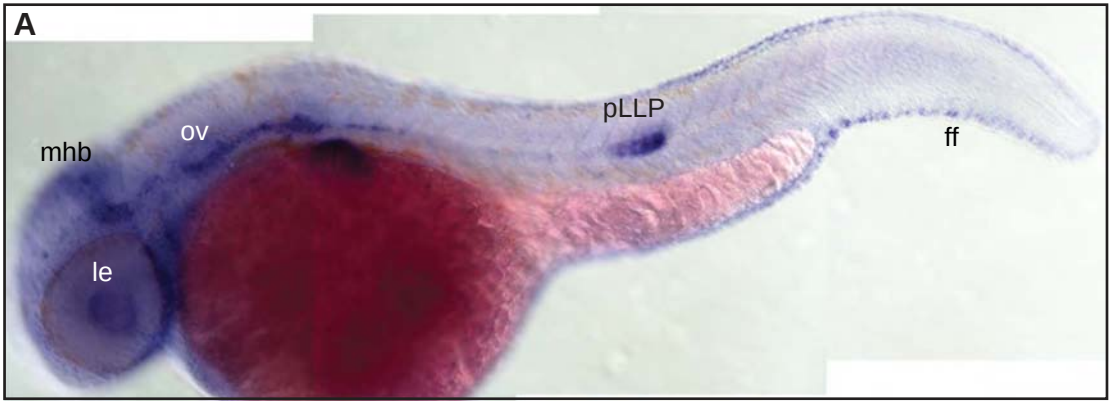

dkk1b

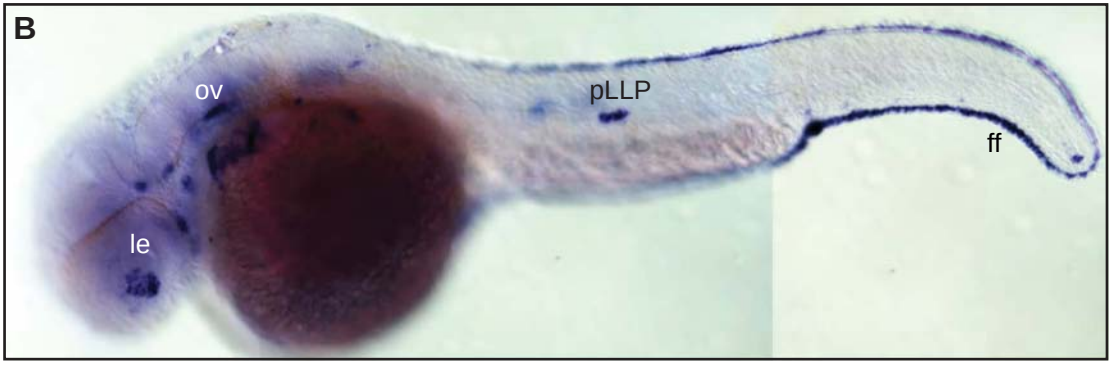

dkk2

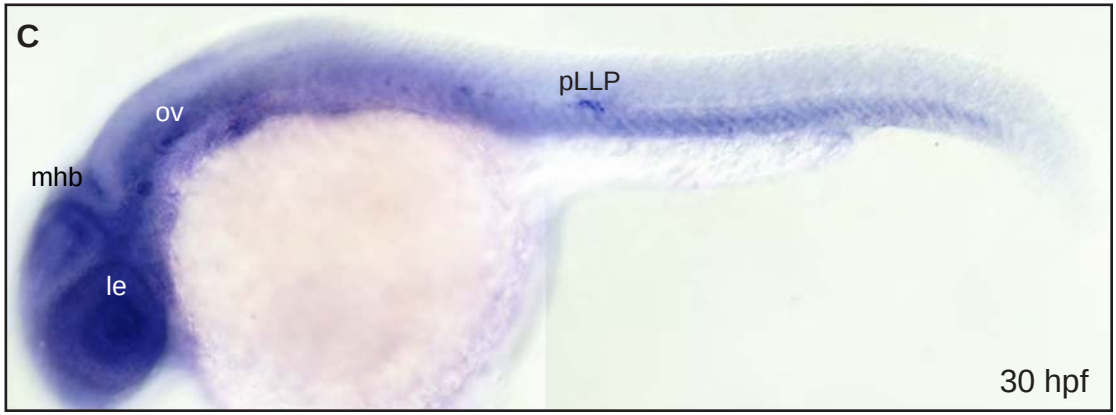

Figure S4

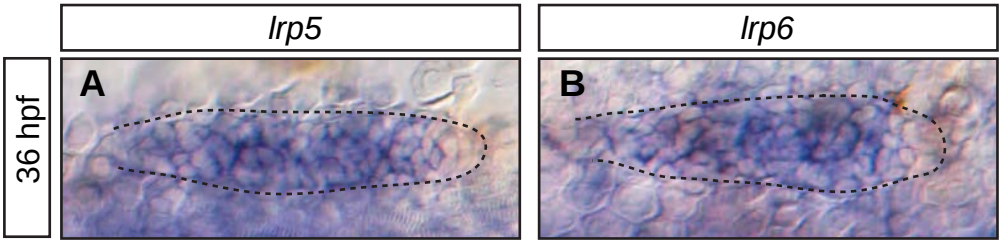

Figure S5

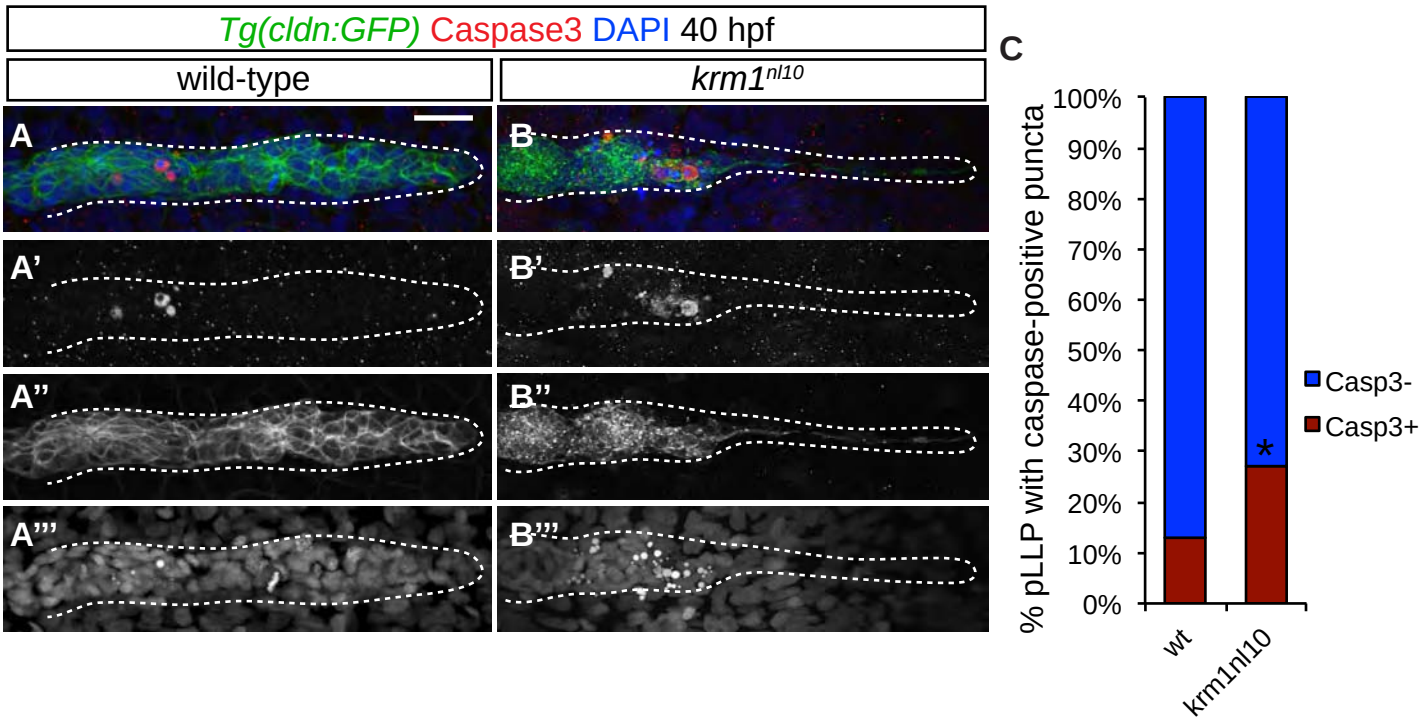
Tg(cldn:GFP) Caspase3 DAPI 40 hpf
wild-type
krm1nl10
A
B
A'
B'
A''
B''
A'''
B'''
C
% pLLP with caspase-positive puncta
100%
90%
80%
70%
60%
50%
40%
30%
20%
10%
0%
Casp3-
Casp3+
*
wt
krm1nl10

Figure S6

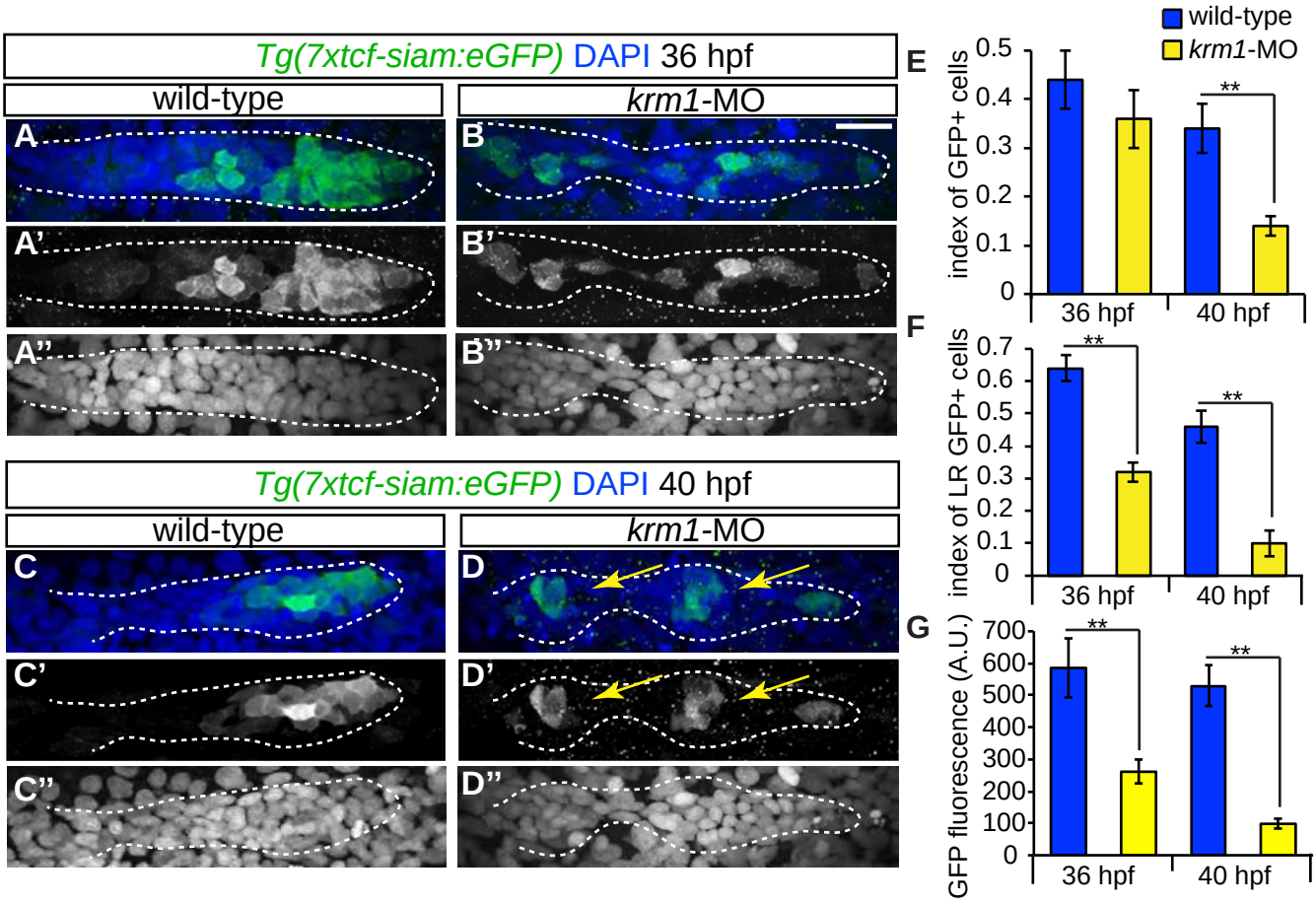
Tg(7xtcf-siam:eGFP) DAPI 36 hpf
wild-type
krm1-MO
A
A'
A''
B
B'
B''
Tg(7xtcf-siam:eGFP) DAPI 40 hpf
wild-type
krm1-MO
C
C'
C''
D
D'
D''
E
wild-type
krm1-MO
index of GFP+ cells
0.5
0.4
0.3
0.2
0.1
0
**
36 hpf
40 hpf
F
index of LR GFP+ cells
0.7
0.6
0.5
0.4
0.3
0.2
0.1
0
**
**
36 hpf
40 hpf
G
GFP fluorescence (A.U.)
700
600
500
400
300
200
100
0
**
**
36 hpf
40 hpf

Figure S7

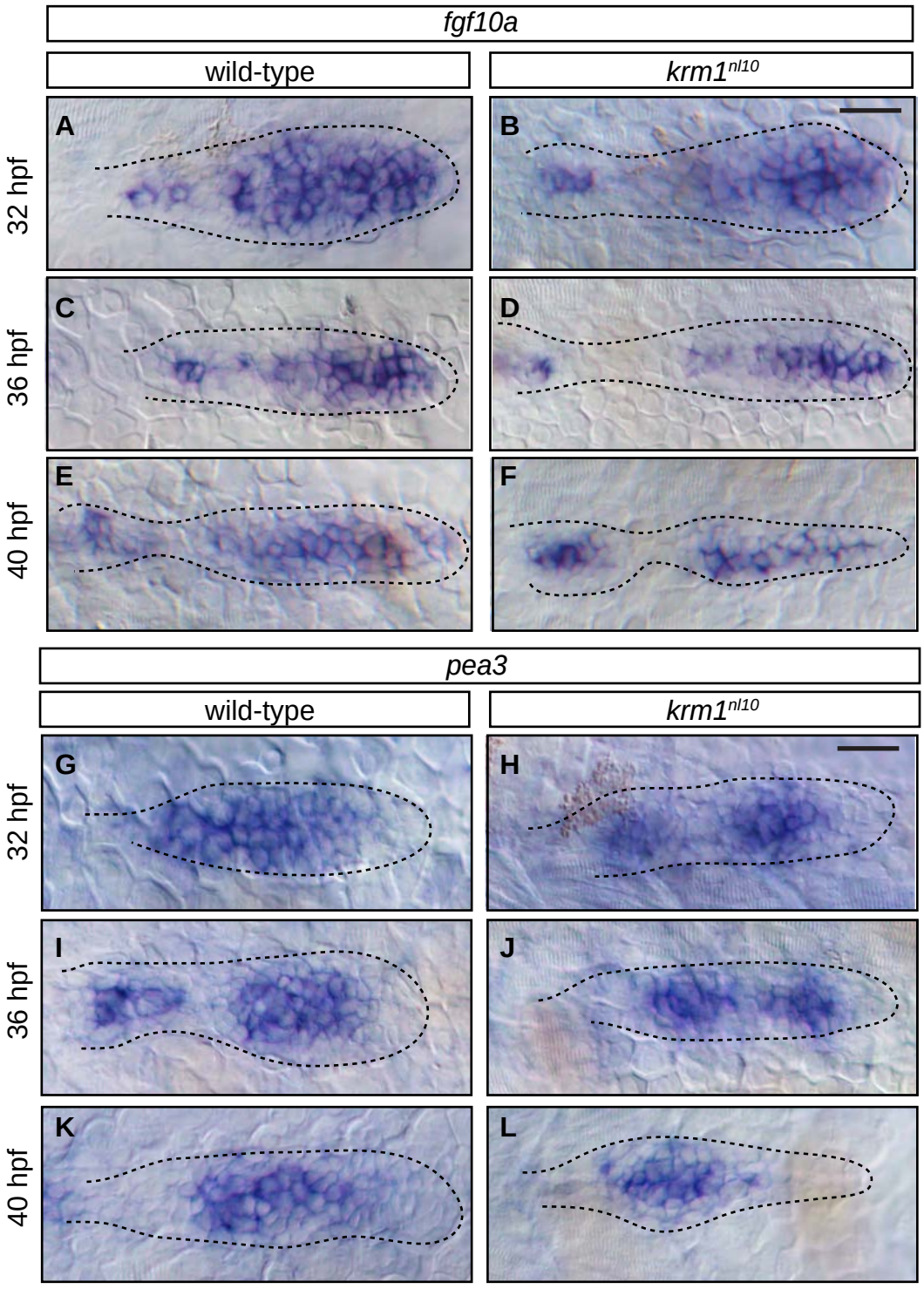
fgf10a
wild-type
krm1nl10
A
B
32 hpf
C
D
36 hpf
E
F
40 hpf
pea3
wild-type
krm1nl10
G
H
32 hpf
I
J
36 hpf
K
L
40 hpf

Figure S8

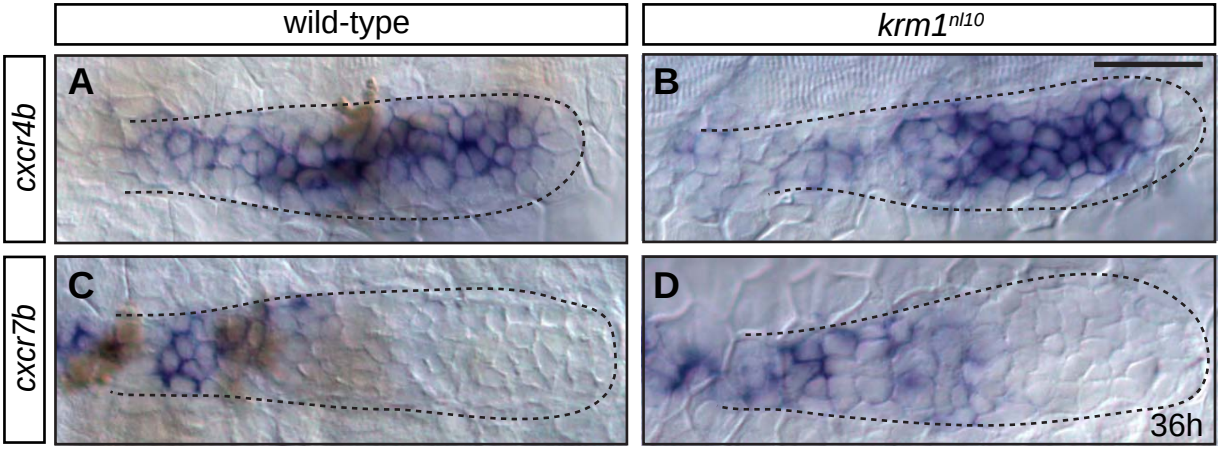

Figure S9

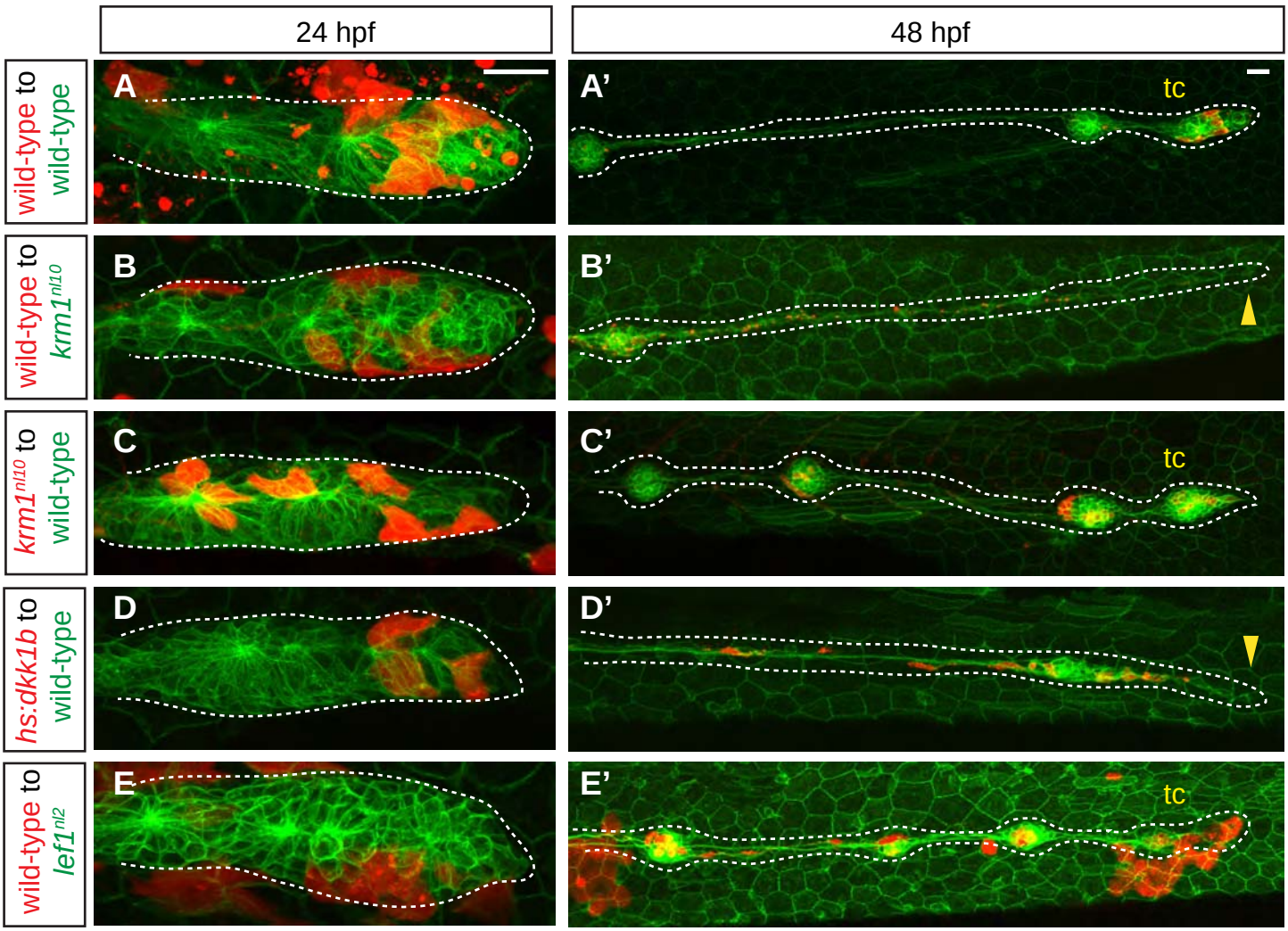
24 hpf
48 hpf
wild-type to wild-type
wild-type to krm1nl10
krm1nl10 to wild-type
hs:dkk1b to wild-type
wild-type to lef1nl2
A
A'
B
B'
C
C'
D
D'
E
E'
tc
tc
tc

Figure S10

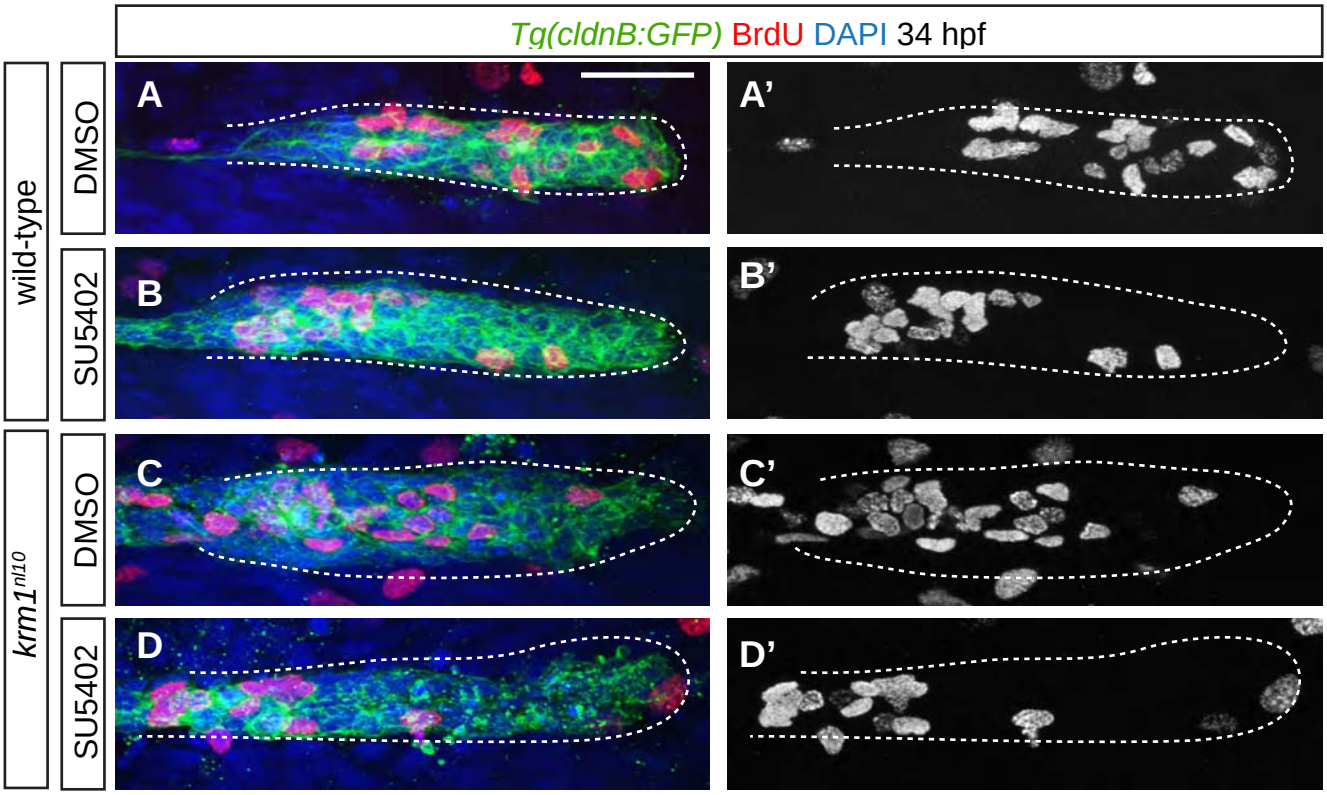
Tg(cldnB:GFP) BrdU DAPI 34 hpf
wild-type
krm1nl10
DMSO
SU5402
DMSO
SU5402
A
A'
B
B'
C
C'
D
D'

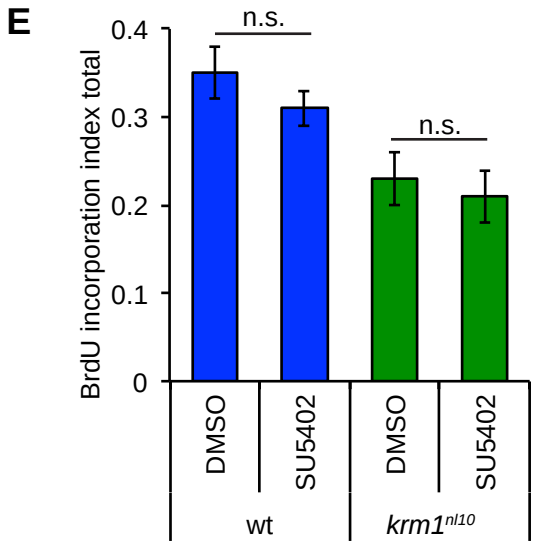
E
BrdU incorporation index total
0.4
0.3
0.2
0.1
0
n.s.
n.s.
DMSO
SU5402
DMSO
SU5402
wt
krm1nl10

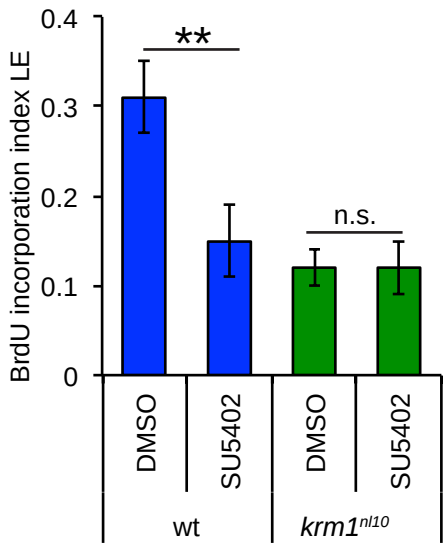
F
BrdU incorporation index LE
0.4
0.3
0.2
0.1
0
**
n.s.
DMSO
SU5402
DMSO
SU5402
wt
krm1nl10

Figure S11

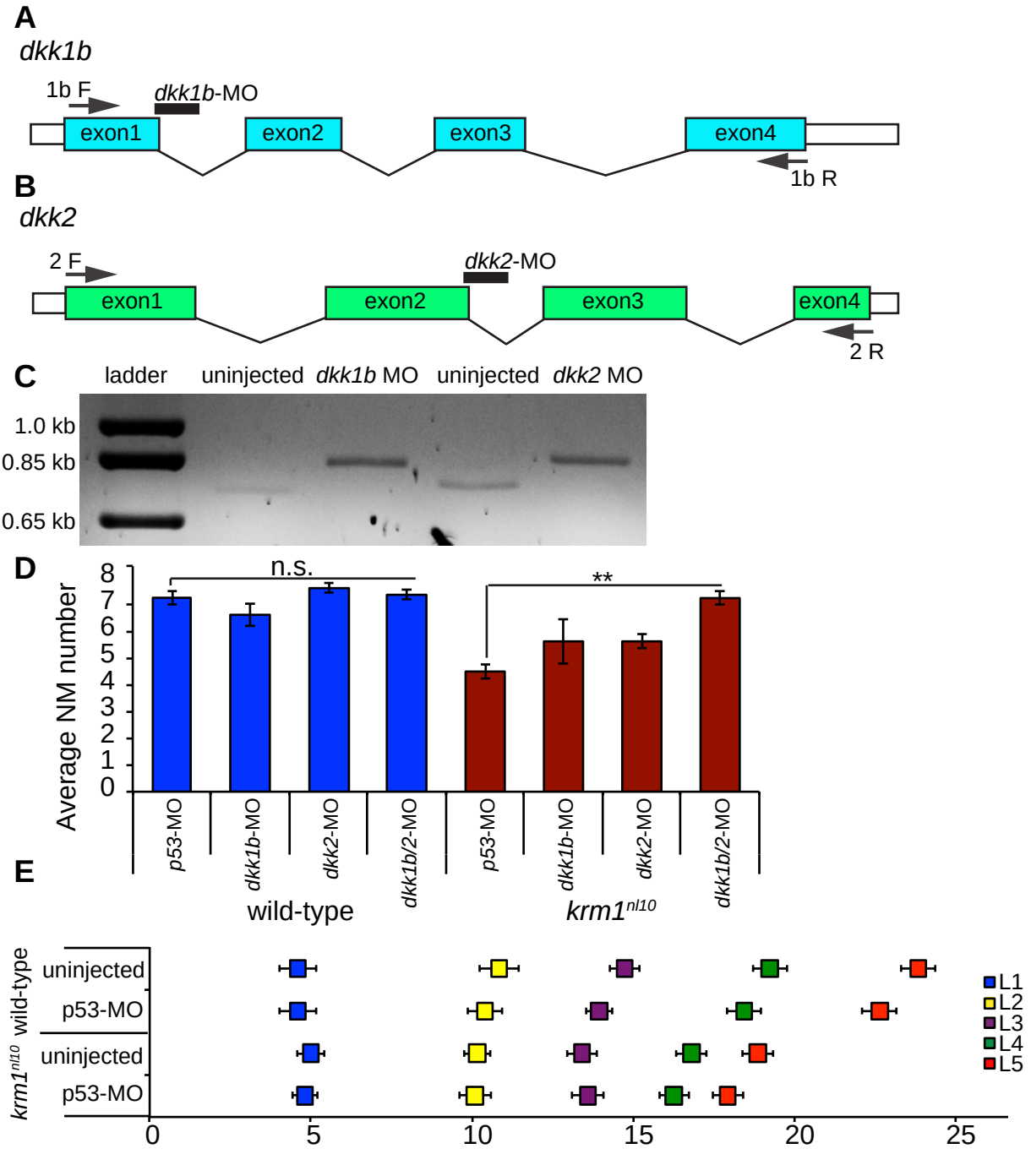
A
dkk1b
1b F
dkk1b-MO
exon1
exon2
exon3
exon4
1b R
B
dkk2
2 F
dkk2-MO
exon1
exon2
exon3
exon4
2 R
C
ladder
uninjected
dkk1b MO
uninjected
dkk2 MO
1.0 kb
0.85 kb
0.65 kb
D
Average NM number
n.s.
**
p53-MO
dkk1b-MO
dkk2-MO
dkk1b/2-MO
wild-type
krm1nl10
E
wild-type
krm1nl10
uninjected
p53-MO
uninjected
p53-MO
L1
L2
L3
L4
L5

Figure S12

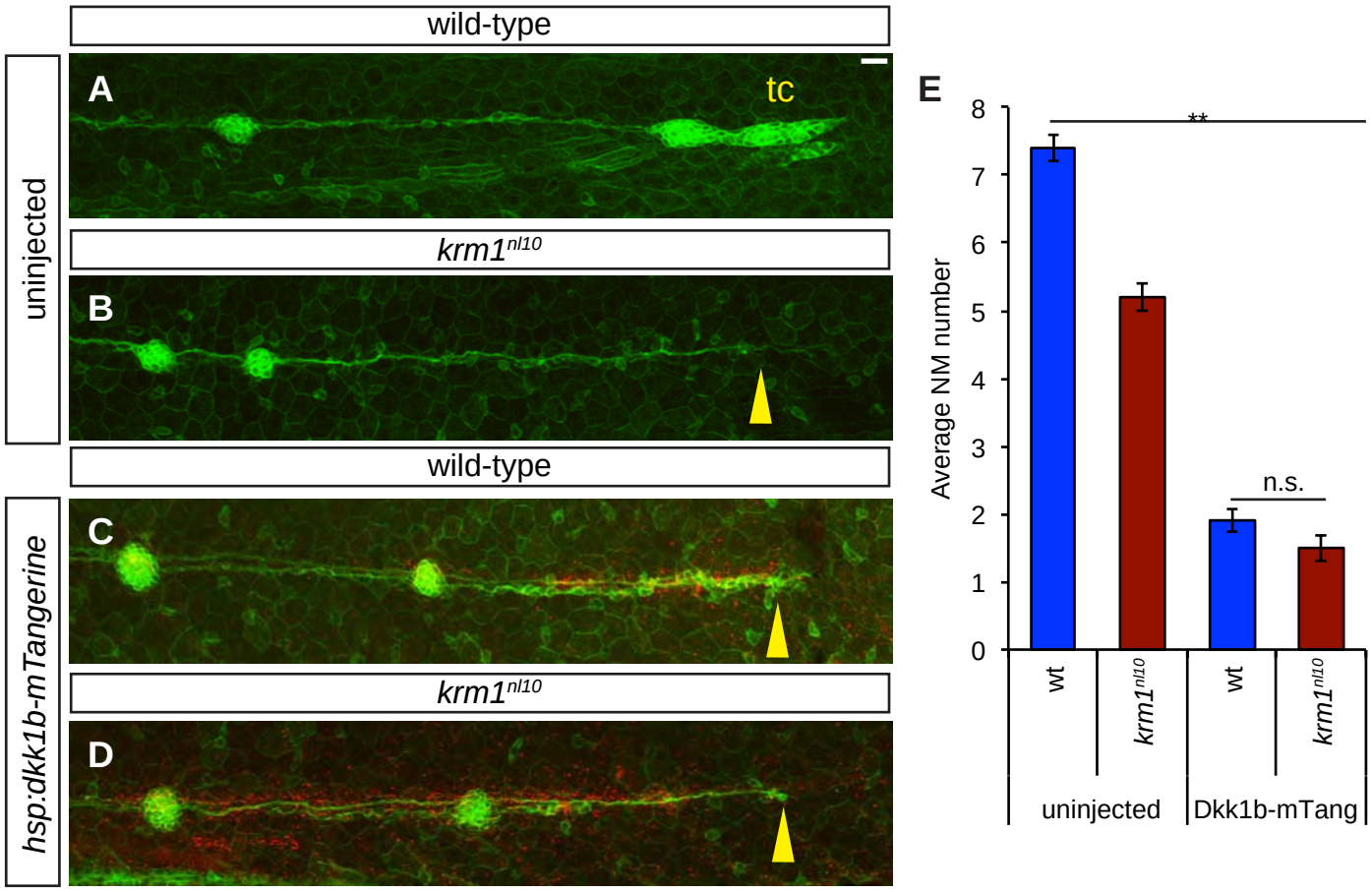

Tg(cldnB:GFP) Dkk1b-mTangerine 2 dpf

Figure S13

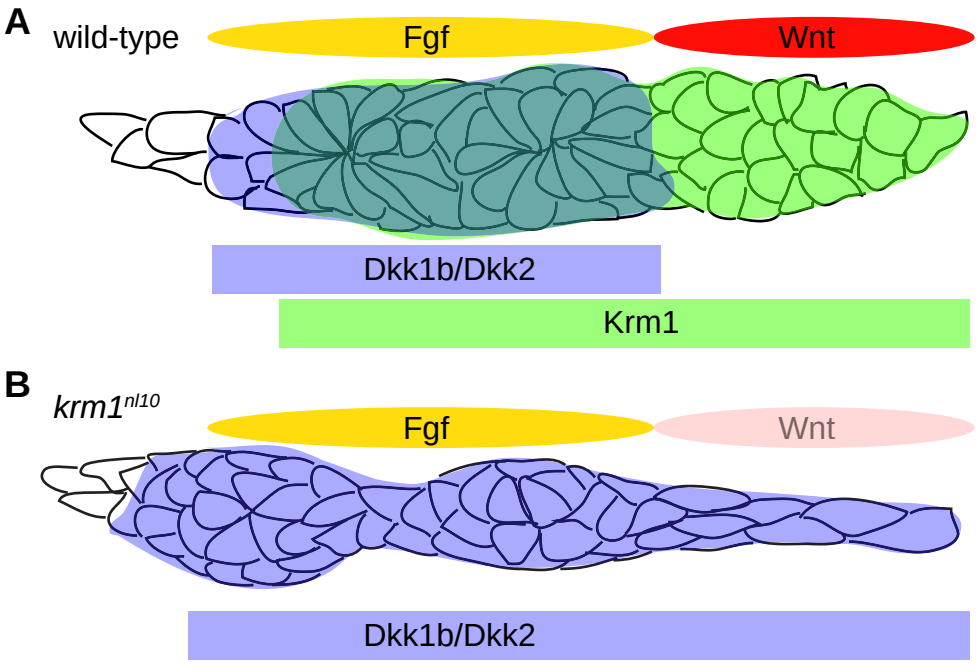
A
wild-type
Fgf
Wnt
Dkk1b/Dkk2
Krm1
B
krm1nl10
Fgf
Wnt
Dkk1b/Dkk2

Supplementary Movie Legends

Movie 1. Wild-type pLLP deposits NMs at regular intervals along the trunk
Time-lapse confocal projections of a *Tg(cldnB:GFP)*-positive wild-type pLLP imaged every 10 minutes for 15.5 hours starting at 36 hpf. During the course of imaging, the pLLP deposits 2 NMs and migrates out of the field to view. Scale bar: 100 μM.

Movie 2. pLLP migration fails in a *krm1*^{nl10} mutant
Time-lapse confocal projections of a *krm1*^{nl10} mutant pLLP labeled by *Tg(cldnB:GFP)* expression. Images were collected every 10 minutes for 15.5 hours beginning at 36 hpf. The mutant pLLP deposits 3 NMs before stalling and extending as a thin trail of cells. Scale bar: 100 μM.

Movie 3. Wnt sensor cells remain in the pLLP during migration
Live time-lapse confocal projections of a mosaic pLLP containing wild-type rhodamine labeled *Tg(7xtcf-siam:eGFP)*-positive and *Tg(7xtcf-siam:eGFP*)-negative donor cells in a wild-type *Tg(neuroD:eGFP)* host. Expression of *Tg(neuroD:eGFP)* marks extending pLL axons. Still images of this embryo at 24 and 48 hpf are shown in Fig. 5E,G. Images were collected every 10 minutes for 9.3 hours beginning at 34 hpf. During the course of migration, both GFP-positive and GFP-negative donors cells migrate along the trunk of the embryo. Scale bar: 100 μM.

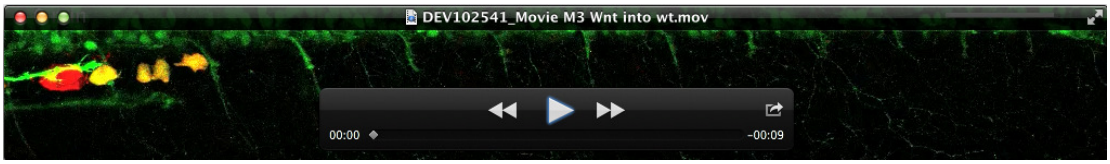

Movie 4. Wild-type donor cells fail to survive in a *krm1*^{nl10} mutant host
Live time-lapse confocal projections of a mosaic pLLP containing wild-type rhodamine labeled *Tg(7xtcf-siam:eGFP)*-positive and *Tg(7xtcf-siam:eGFP*)-negative donor cells in a *krm1*^{nl10} mutant *Tg(neuroD:eGFP)* host. Still images of this embryo at 24 and 48 hpf are shown in Fig. 5F,H. Images were collected every 10 minutes for 9.3 hours beginning at 34 hpf. Note that wild-type donor cells fragment and die (blue arrowhead) in the mutant pLLP during migration. Scale bar: 100 μM.